RSC Advances

PAPER

View Article Online
View Journal | View Issue

Cite this: *RSC Adv.*, 2025, **15**, 17442

Targeted metabolomic profiling and antibacterial assessment of extracts from leaves, stems, and fruits of Egyptian *Parkinsonia aculeata* L.†

Asmaa S. Abd Elkarim, *[a] Tulip A. Medhat,[b] Ahmed F. Essa,[c] Sahar Abdelaziz[d] and Samia S. Hafez[d]

This study investigated the metabolic profiles and antibacterial activities of *Parkinsonia aculeata* leaves, stems, and fruits. Butanol extracts were analyzed using LC-ESI-MS/MS, tentatively identifying 116 secondary metabolites based on fragmentation patterns, biosynthetic pathways, and literature comparisons. Spectral similarity networks generated through the Global Natural Products Social Network (GNPS) revealed chemical similarities and identified 6 uncommon flavone compounds. Spectral similarity analysis revealed a close chemical resemblance between leaves and stems, while fruits exhibited distinct profiles. Antibacterial activity was assessed against seven pathogenic strains using both disk diffusion and microbroth dilution methods. Leaf extracts demonstrated the strongest activity, with inhibition zones up to 20.13 mm and MIC values as low as 1.5 mg mL^{-1}, particularly against *S. aureus* ATCC 29213. Stem extracts showed comparable efficacy, while fruit extracts were more effective against *K. pneumoniae*. These findings highlight *P. aculeata* as a promising natural source of bioactive compounds for potential antimicrobial applications.

Received 7th February 2025
Accepted 8th May 2025

DOI: 10.1039/d5ra00906e

rsc.li/rsc-advances

1 Introduction

Herbal medicines and their derivative products are widely used as therapeutic products in many countries. Their worldwide use has increased in the last decade. There are hundreds of active components in these herbs, and it is almost impossible to identify all these compounds.[1] Various mass spectrometric techniques have been gradually employed for the investigation of medicinal plants to profile their secondary metabolites of plants. Liquid chromatography-electro-spray ionization tandem mass spectrometry (LC-ESI-MS/MS) is a widely recognized method for plant extract metabolite fingerprinting.[2–5] Infectious diseases, primarily caused by bacteria, viruses, rickettsia, and fungi, continue to be significant. Although synthetic antibiotics have been extensively developed to manage these infections, their overuse has contributed to the emergence of antibiotic-resistant strains, creating a serious public health concern. Consequently, there is an urgent need to discover safe and effective antibacterial agents. Natural products derived from plants, particularly those rich in secondary metabolites like flavonoids and tannins, have shown great promise as safer alternatives. Medicinal plants have been traditionally used for generations, valued for their low cost, wide availability, and perceived safety.[6]

Parkinsonia aculeata L., South American native that was, first observed in the wild in Egypt. It was noted during the vegetation survey of Elephantine Island in the Aswan Governorate, then in the Western Desert's Dakhla Oasis. A macromorphological comparison of the gathered specimens with specimens from other countries' herbariums and live specimens grown in Alexandria's Antoniades Botanic Garden verified the species identity.[7] *P. aculeata* L. is a species of the third-largest flowering plant family called Fabaceae. This family contributes important to human society. It has a lot of beneficial species, including woody, medicinal, and vegetable plants. *P. aculeata* is a big, prickly shrub or small tree, that can grow to a height of over 4 meters. This plant is cultivated for its beautiful and exquisite yellow flowers. It also possesses an amazing ability for survival and growth in a variety of soil types and environmental circumstances.[8]

According to the studies of the genus *Parkinsonia*, it contains variable classes of polyphenolic constituents as flavonoids; flavones/falvonols and their glycosides. In addition to terpenoids, saponins, fatty acids, tannins, sterols, alkaloids, and amino acids. *P. aculeata* L. has a number of documented health benefits, including antimalarial (leaves and flowers), smooth muscle stimulant, anti-inflammatory, hepatoprotective (leaves extract), antioxidant, hypoglycemic (aqueous extract of aerial

[a]*Chemistry of Tanning Materials and Leather Technology Department, National Research Centre, Giza 12622, Egypt. E-mail: asmaa_nrc@yahoo.com*
[b]*Obour Health Insurance Organization Clinics, Obour City, Egypt*
[c]*Chemistry of Natural Compounds Department, National Research Center, 33 El Bohouth St., Dokki, Giza 12622, Egypt*
[d]*Department of Pharmacognosy, Faculty of Pharmacy, Zagazig University, Zagazig, 44519, Egypt*

† Electronic supplementary information (ESI) available. See DOI: https://doi.org/10.1039/d5ra00906e

part and bark), antispermatogenic (ethanolic extract of stem bark),[9,10] antimicrobial, analgesic, and antipyretic.[11] Pregnant women may use the boiling aqueous extract of its leaves as an abortifacient., therefore, *P. aculeata* may a herbal medicine.[12]

Under optimized conditions of pH, temperature, and concentration, the ethanol extract of *P. aculeata* has demonstrated promising antibacterial activity against various bacterial infections in biological systems.[13] Moreover, both hexane and methanol extracts have shown significant antibacterial effects at defined concentrations. Similarly, crude leaf extracts obtained using ethanol, petroleum ether, and chloroform exhibited notable inhibitory activity against several bacteria species. The leaves and bark of *P. aculeata* exhibit significant therapeutic benefits for the treatment of various diseases, mainly due to their strong antimicrobial, antibacterial, and antioxidant activities. Polyphenols be responsible for the antimicrobial activity of dried aerial parts and dried stem bark.[14]

In our study we selected the butanol extract of leaves, stems, and fruits from Egyptian *P. aculeata* for antibacterial effects because evaluating its antibacterial potential provides novel insights and contributes valuable data to the scientific literature. Preliminary chromatographic analyses revealed that it is particularly rich in bioactive secondary metabolites, especially polyphenolic compounds, which are known for their strong antimicrobial properties.[15] Moreover, the studies conducted on the Egyptian *P. aculeata* are rare, and did not consider the chemical profiles by LC-ESI-MS/MS of its butanol extract form different organs as well as their antimicrobial effect. This work represents the first comprehensive analysis of the bioactive compounds responsible for the antibacterial efficacy of the butanol extracts from the leaves, stems, and fruits of *P. aculeata*.

Based on the previous therapeutic benefits, antimicrobial effects of *P. aculeata* extracts, and its beneficial bioactive compounds, we maintaining our objective of studying antibacterial potential of butanol extract (BE) from leaves (L), stems (S), and fruits (F) in relation to their chemical profiling. Our current work aimed to (i) utilize LC-ESI-MS/MS analysis along with molecular networking to comprehensively characterize and map the chemical composition of the butanol extracts (BE) from the leaves, stems, and fruits of *P. aculeate* (ii) evaluate the antibacterial activity of the butanol extracts from different plant parts (leaves, fruits, and stems) against selected pathogenic bacteria; and (iii) identify the bioactive constituents responsible for the observed antibacterial effects (Fig. 1).

2 Materials and methods

2.1. Plant-based components

Aerial parts of *P. aculeata* (Fig. 1A) were collected in May 2019, during the plant's flowering period, from the Orman Botanical Garden, Dokki, Giza, Egypt. The species was taxonomically identified by Dr M. El-Gibaly, Lecturer of Taxonomy and Consultant for the Central Administration of Plantation and Environment. A voucher specimen (No. T79) was deposited at the Chemistry of Tanning Materials and Leather Technology Department, National Research Centre, Dokki, Cairo, Egypt. As the plant was cultivated as an ornamental tree within the botanical garden, no special permit was required for its collection. The authors confirm that no protected or endangered species were involved in this study. After collection, the plant samples were thoroughly cleaned to remove dust, air-dried in the shade for 15 days, and then ground into a fine powder using a grinder (IKA® MF 10 Basic Microfine Grinder Drive, Breisgau, Germany). The powdered samples were stored in paper bags in the refrigerator until further analysis.

2.2. Chemicals and drugs

Di-ionized water (DI-H_2O) is further purified using the Milli-Q Plus water purification equipment from Millipore Ltd in Bedford, Massachusetts, as well as analytical-grade (CH_3OH, acetonitrile; CAN, formic acid) and HPLC DMSO from Merck in

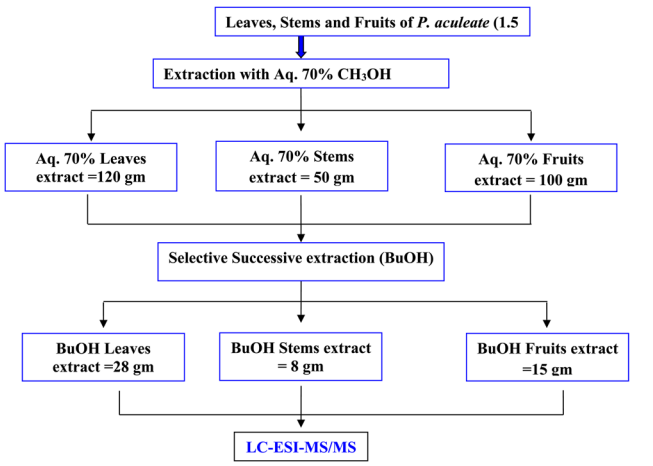

Scheme 1 Extraction and fractionation of *P. aculeata* leaves (L), stems (S), and fruits (F).

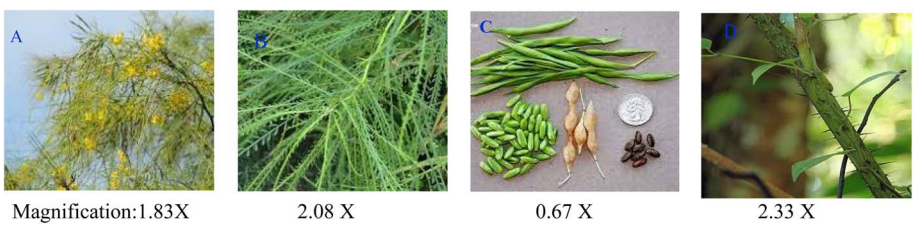

Fig. 1 *P. aculeata* tree (A); leaves (B), fruits (C), and stems (D).

Darmstadt, Germany. The following substances were bought from Sigma Chemical Co.

2.3. Extraction method and fractionation

Air-dried and powdered leaves (L), stems (S), and fruits (F) of *P. aculeata* (1.5 kg each) were separately extracted with 70% aqueous methanol ($CH_3OH : H_2O$) under reflux at 60 °C. Each plant part was extracted in five successive batches (5 × 6 L) until complete exhaustion, as monitored by thin-layer chromatography (TLC). The combined extracts for each part were filtered and concentrated under reduced pressure at 50 °C using a rotary evaporator, yielding crude methanolic residues: approximately 120 g from the leaves, 50 g from the stems, and 100 g from the fruits. Each dried residue was suspended in a mixture of methanol and water ($CH_3OH : H_2O$, 1 : 9, v/v; 300 mL) and subjected to successive liquid–liquid partitioning with solvents of increasing polarity: petroleum ether (60 : 80), chloroform ($CHCl_3$), ethyl acetate (EtOAc), and *n*-butanol (*n*-BuOH) (Scheme 1). After solvent partitioning, the obtained fractions were as follows: petroleum ether fraction: 5 g (L), 0.5 g (S), and 2.5 g (F); chloroform fraction: 7 g (L), 2 g (S), and 5 g (F); ethyl acetate fraction: 16 g (L), 5.5 g (S), and 9.5 g (F); *n*-butanol fraction: 28 g (L), 8 g (S), and 15 g (F).[9]

Preliminary chromatographic profiling (TLC and HPLC) revealed that the ethyl acetate and *n*-butanol fractions were rich in polyphenolic compounds, whereas the petroleum ether and chloroform fractions showed a low content of these metabolites. Based on these findings, the *n*-butanol fractions were selected for further phytochemical investigation by LC-ESI-MS/MS analysis.

2.4. Sample preparation for HPLC profiling and MS analysis

The lyophilized BuOH extracts of the three organs (50 mg each) were adequately dissolved in 70% CH_3OH (HPLC-grade) with sonication (10 min), and particulate matter was removed, allowing for a clearer sample for analysis, then centrifuged. After evaporating the aliquots under reduced pressure, they were freeze-dried for 48 hours. About 10 mg of the dried BuOH extracts were dissolved in 500 mL of CH_3OH (HPLC-grade), each in triplicates, and 10 mL were injected for HPLC profiling. For the MS/MS analysis, three copies of 10 mg in 250 mL of CH_3OH (MS-grade) were prepared using 5 mL as the injection volume in the LC-MS/MS analysis.[5]

2.5. Equipment and conditions

2.5.1. HPLC/ESI-MS/MS analysis. The sample was analyzed using liquid chromatography-electrospray ionization tandem mass spectrometry (LC-ESI-MS/MS) with a SCIEX Triple Quad 5500+ MS/MS system fitted with an electrospray ionization (ESI) detector for detection and an Exion LC AC system for separation. Ascentis® C18 Column (4.6 × 150 mm, 3 μm) was used for the separation. The mobile phases included two eluents: acetonitrile (HPLC-grade) and 0.1% formic acid (A). The gradient of mobile phase was set up as follows: 0% B at 0–2 minutes, 10% at 36.1, 10% from 36.1–40 minutes, 90% at 2–30 minutes, and 90% at 30–36 minutes. The flow rate was 0.7 mL min^{-1}, while 10 μL was the injection volume. With a scan (EMS-IDA-EPI) from 100 to 1000 Da for MS1, negative ionization mode (−ve) was used for MS/MS analysis with the following parameters: ion spray voltage: −4500; source temperature: 500 °C; curtain gas: 25 pressure; ion source gas 1 and 2 were 45 psi and ranged from 50 to 1000 Da for MS2, with a collision energy of −35 and a collision energy spread of −80. The MS-DIAL software version 4.70 and the Fiehn HILIC library were used to identify the constituents.

2.6. Molecular networking

The raw data files generated from LC-ESI-MS/MS analysis were converted into mzXML format using the MS Convert tool from ProteoWizard (version 3.0.21050, **https://www.proteowizard.org**). Once converted, the data were uploaded to the MassIVE Data sets repository *via* WinSCP (**https://www.massive.ucsd.edu**). Molecular networking (MN) of the LC-ESI-MS/MS data was performed using the Global Natural Product Social (GNPS) platform. The analysis parameters included a mass tolerance of 0.2 Da for precursor ions and 0.05 Da for fragment ions, adhering to the default GNPS settings. A minimum of six MS fragments was required to establish matches between consensus MS/MS spectra, with a cosine score threshold of 0.7 set to define similarity between nodes. The resulting molecular network was exported as a GraphML file and visualized using a force-directed layout in Cytoscape version 3.7.1, following methods detailed in prior studies.[16,17]

2.7. Antibacterial assay of *P. aculeata* extracts (leaves, stems, and fruits)

2.7.1. Bacterial strains. All bacterial strains, including the standard strains [*Staphylococcus aureus* ATCC 29213 (*S. aureus*), *Pseudomonas aeruginosa* ATCC 27853 (*P. aeruginosa*), *Escherichia coli* ATCC 25922 (*E. coli*)] and clinical isolates of *S. aureus*, *P. aeruginosa*, and *E. coli*, were sourced from the American Type Culture Collection (ATCC) in Rockville, MD, USA, and the Northern Utilization Research and Development Division of the United States Department of Agriculture (NRRL) in Peoria, IL, USA. Before conducting the bioassay, the bacterial strains were rejuvenated by sub-culturing them in a fresh nutrient broth medium for 24 hours. This assay was performed at the Regional Centre for Mycology and Biotechnology, Al-Azhar University, Cairo, Egypt.

2.7.2. Biological assessment

2.7.2.1. Disk diffusion assay. The antibacterial activity of *P. aculeata* extracts (leaves, stems, and fruits) was evaluated using the disk diffusion method.[18] Bacterial strains were initially cultured on Mueller–Hinton agar, except for *Streptococcus*, which was grown on Mueller–Hinton agar enriched with 50 mL L^{-1} blood, at 37 °C for 24 hours before being transferred to nutrient agar. Sterile filter disks (6 mm in diameter, Whatman no. 3) were placed on agar plates inoculated with the bacterial suspension. Each disk was treated with 40 μL of the extract dissolved in 60% ethanol at various concentrations (2.00 mg mL^{-1}, 1.00 mg mL^{-1}, 0.50 mg mL^{-1}). The prepared Petri dishes

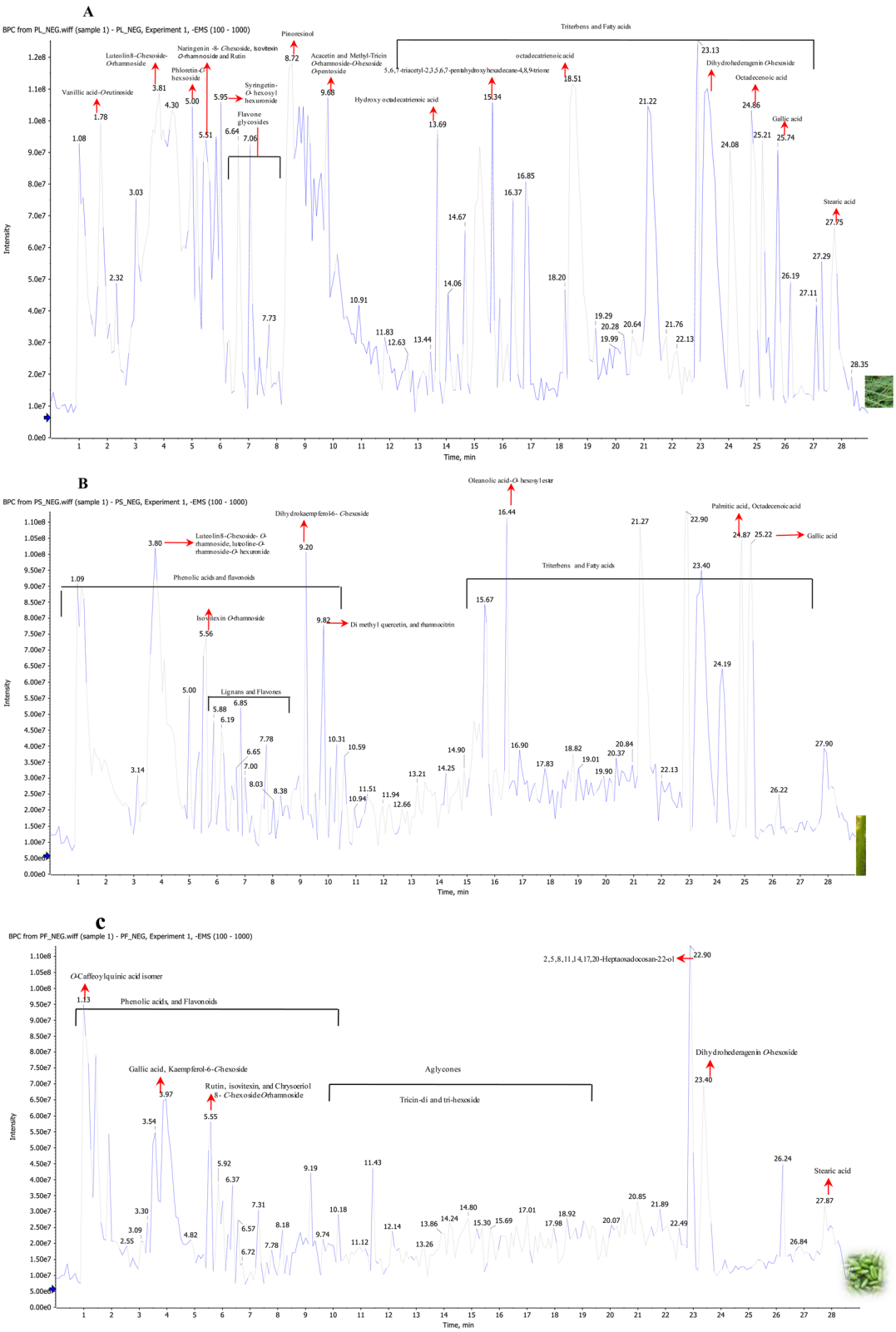

Fig. 2 Total ion current chromatogram (TIC), and (B): base peak intensity chromatograms of *P. aculeata* butanol extracts from (A): leaves, (B): stems and (C): fruits using HPLC-ESI-MS/MS in (−ve) ionization mode.

were stored at 4 °C for 1 hour and then incubated at 37 °C for 24 hours. Standard disk of vancomycin (30 μg) was used as reference control. Antibacterial activity was determined by measuring the inhibition zones around the disks. All experiments were conducted in triplicate, and the results were presented as mean ± standard deviation (SD).

Table 1 Metabolites detected in the butanol extracts of leaves, stems and fruits from *P. aculeata* using HPLC-ESI-MS/MS in negative (−ve) ionization mode[a]

Peak no.	R_t (min)	Tentatively identified compounds	Mol. ion *m*/*z* ppm (−)	MS^2 major production	Organs		
					Leaf	Stem	Fruit
Phenolics							
1	0.36	Cinnamic acid	146.90	102.95 $[M-H-COO]^-$, 129.21 $[M-H-H_2O]^-$, 118.88, 100.81	+	+	+
2	0.852	Protocatechuic aldehyde	137.00	121.08, 108.48 $[M-H-CHO]^-$, 109.07 $[M-H-CO]^-$, 101.86 $[M-H-2H_2O]^-$	−	+	−
3	1.013	Citric acid	191	129$[M-H-COO-H_2O]^-$, 110.94 $[M-H-COO-2H_2O]^-$	−	−	+
4	1.033	Quinic acid	191	163.10 $[M-H-CO]^-$, 146.99 $[M-H-COO]^-$, 145.08 $[M-H-CO-H_2O]^-$, 118.97, 110.99 $[M-H-COO-2H_2O]^-$	+	−	+
5	1.127	*O*-Caffeoylquinic acid isomer	353.09	191.06 [M-H-caffeoyl (162)]$^-$, 179.03 [M-H-quinate (174)]$^-$, 173.03	+	+	+***
6	1.160	Caffeic acid	179.08	161.06 $[M-H-H_2O]^-$, 135.05 $[M-H-COO]^-$, 121.04, 111.01, 107.03	+	+	+
7	1.432	Caffeic acid hexoside	341.10	323.17 $[M-H-H_2O]^-$, 297.19 $[M-H-COO]^-$, 179.03 [M-H-162(hex)]$^-$, 135.05 [M-H-162(hex)-COO]$^-$, 134.02, 119.04	+	+	+
8	1.555	Ferulic acid	192.99	174.98 $[M-H-H_2O]^-$, 156.94 $[M-H-2H_2O]^-$, 149.04 $[M-H-COO]^-$, 134.05, 133.05, 137.01, 117.00	+	+	+
9	1.666	Methyl gallate *O*-hexoside	345.10	183.11 [M-H-162(hex)]$^-$, 168.03 [M-H-162(hex)-CH_3]$^-$, 137.12 [M-H-162(hex)-H_2O-OCH_3]$^-$	−	+	−
10	1.783	Vanillic acid-*O*-rutinoside	475.00	167.05 [M-H-308(rut)]$^-$, 123.06	−	+	+
11	1.872	Hydroxy-anthranilic acid	154.06	137.04, 135.96 $[M-H-H_2O]^-$, 117.95 $[M-H-2H_2O]^-$, 110.05 $[M-H-CO_2]^-$, 108.03 $[M-H-COOH]^-$	−	−	+
12	1.897	Vanillic acid-*O*-hexoside	329.00	167.05 [M-H-162(gl)]$^-$, 123.11 [M-H-162(gl)-COO]$^-$	−	−	+
13	2.223	Vanillic acid	167.01	149.03 $[M-H-H_2O]^-$, 123.02 $[M-H-COO]^-$, 121.02, 107.02, 105.02 $[M-H-H_2O-COO]^-$, 111.02, 116.91	−	+	+
14	2.398	Coumaric acid hexuronide	339.24	163.07 [M-H-176(gluc)]$^-$	+	+	−
15	2.489	*P*-Hydroxy benzoic acid	137.00	136.05, 116.95, 118.99 $[M-H-H_2O]^-$, 109.04 $[M-H-CO]^-$, 108.01, 101.92, 93.00 $[M-H-COO]^-$	+	−	−
16	2.660	Coumaric acid di-*O*-hexuronide	515.17	339.21[M-H-176(gluc)]$^-$, 163.19 [M-H-352(di gluc)]$^-$	+	+	−
17	2.972	Protocatechueic acid	153.00	135.01 $[M-H-H_2O]^-$, 116.92 $[M-H-2H_2O]^-$, 109.01 $[M-H-COO]^-$	+*	+	+
18	2.983	Coumaric acid	163.10	144.92 $[M-H-H_2O]^-$, 147.12, 135.03, 119.03 $[M-H-COO]^-$, 121.06, 117.00 $[M-H-HCOOH]^-$	+*	+	+
19	3.964	Gallic acid	168.88	151.89, 150.92 $[M-H-H_2O]^-$, 132.94 $[M-H-2H_2O]^-$, 125.05 $[M-H-COO]^-$, 120.94, 108.00	+	+	+**
20	3.377	*p*-Hydroxybenzoic acid-4-*O*-hexoside	298.96	255.05 $[M-H-COO]^-$, 237.03 $[M-H-COO-H_2O]^-$, 137.02 [M-H-162(hex)]$^-$, 119.15 [M-H-162(hex)-H_2O]$^-$, 121.07, 109.08	+	−	−
21	4.128	4-Vinylphenol	118.90	100.80 $[M-H-H_2O]^-$, 101.88	+	−	−
22	6.774	Methyl gallate	183.12	168.90 $[M-H-CH_3]^-$, 150.94 $[M-H-CH_3-H_2O]^-$, 140.00 $[M-H-COCH_3]^-$, 137.04, 123.99 $[M-H-CH_3-CO_2]^-$, 118.04, 111.01, 108.97	+	−	−

Table 1 (*Contd.*)

Peak no.	R_t (min)	Tentatively identified compounds	Mol. ion *m*/*z* ppm (−)	MS^2 major production	Organs		
					Leaf	Stem	Fruit
Flavonols							
23	1.438	Kaempferol-*O*-rhamnoside	430.93	285.12 $[M-H-146(rham)]^-$, 241.11, 223.08, 193	+	–	–
24	3.869	Kaempferol-6-*C*-hexoside	446.90	357.01 $[M-H-90]^-$, 339. 09 $[M-H-90-H_2O]^-$, 327.07 $[M-H-120]^-$, 299.05, 285.10	+	–	+**
25	4.069/9.20 (S)	Dihydrokaempferol-6-*C*-hexoside	448.93	359.03 $[M-H-90]^-$, 329.07 $[M-H-120]^-$, 341.08 $[M-H-90-H_2O]^-$, 301.16, 299.08	+**	–	–
		Dihydrokaempferol-6-*C*-hexoside	459.06, (adduct formate)	449.03 $[M-H-HCOOH]^-$, 431.91 $[M-H-HCOOH-H_2O]^-$, 359.05 $[M-H-HCOOH-90]^-$, 329.06 $[M-H-HCOOH-120]^-$	+	+**	–
26	5.550	Quercetin-3-*O*-rutinoside	608.95	301.14 $[M-H-308(rutinose)]^-$, 300.12	+**	+**	+**
27	5.967	Syringetin-*O*-hexosyl hexuronide	683.01	521.04 $[M-H-162(hex)]^-$, 506.05, 345.23 $[M-H-162(hex)-176(gluc)]^-$, 327.23 $[M-H-162(hex)-176(gluc)-H_2O]^-$, 313.20, 299.13, 341.13, 329.18	–	*+	–
28	6.090	Dimethylquercetin 7-*O*-pentoside-8-*C*-hexoside	622.95	491.11 $[M-H-132]^-$, 460.59 $[M-H-132-2CH_3]^-$, 341.08 $[M-H-132-2CH_3-120]^-$, 314.11, 315.10	+**	–	–
29	6.318	Isorhamnetin-8-*C*-hexoside	477.06	386.93 $[M-H-90]^-$, 356.94, $[M-H-120]^-$, 329.16, 315.00	+	+	+
30	6.565	Isorhamnetin-*O*-pentosyl hexuronide	623.02	491.06 $[M-H-132]^-$, 315.11 $[M-H-132-176]^-$	+	–	–
31	6.600	Dihydro methyl quercetin-7-*O*-pentoside	463.10	331.12 $[M-H-132]^-$, 301.06 $[M-H-132-2CH_3]^-$, 300.06, 282.98, 229.16, 249.10, 342.79	+	–	–
32	6.601	Quercetin-8-*C*-hexoside	463.10	372.87 $[M-H-90]^-$, 342.97 $[M-H-120]^-$	+	+	–
33	6.743	Kaempferol-8-*C*-hexoside	446.90	357.03 $[M-H-90]^-$, 327.03 $[M-H-120]^-$, 285.00, 284, 299.02	+	–	+
34	6.758	Dimethylquercetin di-*O*-hexoside	653.05	491.09 $[M-H-162(hex)]^-$, 329.17 $[M-H-324(dihex)]^-$, 315.13 $[M-H-324(dihex)-CH_3]^-$	+	+	+
35	7.001	Isokaempferide	298.96	283.96 $[M-H-CH_3]$, 269.00 $[M-H-OCH_3]$, 255.99, 172.94, 166.96	+	–	+
36	7.346	Dimethylquercetin-*O*-hexoside	490.95	329.05 $[M-H-162]^-$, 314.13 $[M-H-162-CH_3]^-$, 313.12, 299.03 $[M-H-162-2CH_3]^-$, 285.03	+	+	+
37	8.398	Quercetin 7-*O*-rhamnoside-3-*O*-hexuronide	623.05	477.10 $[M-H-146(rhamn)]^-$, 447.08 $[M-H-176(gluc)]^-$	+	–	+
38	8.687	5,7,3′,4′-Tetra-methyl flavonol	359.10	329.11 $[M-H-2CH_3]^-$, 314.03 $[M-H-3CH_3]^-$, 299.00 $[M-H-4CH_3]^-$	–	+	–
39	9.759	Di methyl quercetin	329.0	314.04 $[M-H-CH_3]^-$, 298.96 $[M-H-2CH_3]^-$, 271.01	+	+	+
40	9.769	(Kaempferide) (rhamnocitrin)	298.95	284.00 $[M-H-CH_3]^-$, 255.24, 227.28, 151.14, 107.25	+	+	+
41	10.530	Syringetin-*O*-hexosyl pentoside	639.08	477.14 $[M-H-hex(162)]^-$, 345.15 $[M-H-162(hex)-132(pent)]^-$, 327.23 $[M-H-162(hex)-132(pent)-H_2O]^-$, 311.24	+	+	+

Table 1 (*Contd.*)

Peak no.	R_t (min)	Tentatively identified compounds	Mol. ion *m*/*z* ppm (−)	MS^2 major production	Organs		
					Leaf	Stem	Fruit
Flavones							
42	1.529	Luteolin 6,8-di-*C*-hexoside	608.95	591.065 $[M-H-18(H_2O)]^-$, 518.94 $[M-H-90]^-$, 488.98 $[M-H-120]^-$, 428.91 $[M-H-180]^-$, 399.10 $[M-H-210(90+120)]^-$, 369.05 $[M-H-240(120+120)]^-$	+	+	−
43	2.291	Chrysoeriol 6,8-di-*C*-hexoside	623.01	533.06 $[M-H-90]^-$, 503.05 $[M-H-120]^-$, 383.04 $[M-H-240]^-$, 413.05 $[M-H-120-90]^-$	+	+	−
44	2.293	Apigenin 6,8-di-*C*-hexoside (vicenin 2)	592.99	503.11 $[M-H-90]^-$, 473.10 $[M-H-120]^-$, 383.20 $[M-H-90-120]^-$, 413.20 $[M-H-180]^-$	+	+	+
45	3.011	Diosmetin 8-*C*-hexoside 6-*C*-pentoside	592.99	575.03 $[M-H-18]^-$, 533.04 $[M-H-60]^-$, 503.00 $[M-H-90]^-$, 473.03 $[M-H-120]^-$, 413.01 $[M-H-180(120+60)]^-$, 383.07 $[M-H-210(90+120)]^-$	+	+	+
46	3.013	Luteolin-*C*-hexoside-*C*-pentoside	578.93	488.96 $[M-H-90]^-$, 458.92 $[M-H-120]^-$, 369.08 $[M-H-90-120]^-$, 399.03 $[M-H-60-120]^-$, 411.05	+	+	+
47	3.466	Tetrahydroxyl dihydroflavone 8-*C*-hexoside	449.30	358.99, 357.03 $[M-H-90]^-$, 329.06 $[M-H-120]^-$, 299.01, 297.07, 133.06	−	+	−
48	3.767	Luteoline-*O*-rhamnoside-*O*-hexuronide	607.00	284.98, 243.05, 257.04	−	+*	−
49	3.809	Luteolin8-*C*-hexoside-*O*-rhamnoside	592.99	473.02 $[M-H-120]^-$, 357.18 $[M-H-90-146(rham)]^-$, 327.18 $[M-H-120-146(rham)]^-$, 383.13 $[M-H-90-120]^-$, 309.21	+	+***	+
50	4.521	Acacetin-*O*-hexoside	445.03	283.06 $[M-H-162(hex)]^-$, 150.04	−	+	−
51	5.232	Apigenin-8-*C*-hexoside (vitexin)	431.01	340.98 $[M-H-90]^-$, 311.04 $[M-H-120]^-$, 283.02 [Ag + 14], 269.00	+	+	+
52	5.428	Luteolin 8-*C*-hexoside-di-*O*-rhamnoside	739.01	593.04 $[M-H-146(rham)]^-$, 575.05, $[M-H-146(rham)-H_2O]^-$, 473.24 $[M-H-146(rham)-120]^-$, 327.52 $[M-H-292(di\ rham)-120]^-$, 285.01 $[M-H-292(di\ rham)-162(hex)]^-$	+	−	−
53	5.479	Isovitexin *O*-rhamnoside	576.99	456.97 $[M-H-120]^-$, 413.04 $[M-H-146(rham)-H_2O(18)]^-$, 341.21 $[M-H-90-146]^-$, 323.20 $[M-H-90-146(rham)-H_2O(18)]^-$, 293.02 $[M-H-120-146(rham)-H_2O(18)]$	+	+	+
54	5.636	Apigenin-6-*C*-hexoside (isovitexin)	430.99	341.03 $[M-H-90]^-$, 323.100 $[M-H-90-H_2O]^-$, 311.10 $[M-H-120]^-$, 283.10 [Ag + 14], 269.04	+	+	−
55	5.670	Chrysoeriol 8-*C*-hexoside*O*-rhamnoside	606.98	486.96 $[M-H-120]^-$, 442.98 $[M-H-146-18(H_2O)]^-$, 341.16 $[M-H-120-146(rham)]^-$, 323.18 $[M-H-120-146(rham)-18(H_2O)]^-$, 308 $[M-H-120-146(rham)-18(H_2O)-CH_3]^-$	*+	−	+
56	6.297	Diosmetin-6-*C*-hexoside	460.99	370.98 $[M-H-90]^-$, 353.08 $[M-H-90-18(H_2O)]^-$, 341.02 $[M-H-120]^-$	+	−	−
57	6.365	Pinocembrin-di-*O*-hexoside	579.01	417.09 $[M-H-162(hex)]^-$, 254.98 $[M-H-324(dihex)]^-$	−	−	+

Table 1 (*Contd.*)

Peak no.	R_t (min)	Tentatively identified compounds	Mol. ion *m*/*z* ppm (−)	MS^2 major production	Organs		
					Leaf	Stem	Fruit
58	6.417	Diosmetin-8-*C*-hexoside	460.98	371.01 $[M-H-90]^-$, 341.05 $[M-H-120]^-$, 299.05, 165.15, 313.21	+	+	+
59	6.603	luteolin7-*O*-rutinoside	593.06	285.03 $[M-H-308(hex + rham)]^-$	−	+	−
60	6.984	Diosmetin *O*-pentosyl hexuronide	607.06	475.05 $[M-H-pentose\ (132)]^-$, 298.99 $[M-H-pentose\ (132)-hexuronide\ (176)]^-$, 284.05 $[M-H-pentose\ (132)-hexuronide\ (176)-CH_3]^-$	−	−	+
61	6.998	Lutoline-6-*C*-hexoside (isoorientin)	447.01	357.04 $[M-H-90]^-$, 339.06 $[M-H-90-H_2O]^-$, 327.10 $[M-H-120]^-$, 285.05, 297.92, 299.06	+	+	+
62	7.159	Diosmetin-*O*-hexoside	460.95	298.96 $[M-H-162(hex)]^-$, 284.00 $[M-H-162(hex)-CH_3]^-$, 283.05	+	+	+
63	7.734	Tricin-*O*-hexuronide	505.00	329.14 $[M-H-176(gluc)]^-$	−	+	+
64	7.953	Pinocembrin-*O*-hexoside	416.98	387.02, 371.11, 343.20, 255.05 $[M-H-162(hex)]^-$, 209.19 $[M-H-162(hex)-2H_2O]^-$	+	−	+
65	8.207	Tricin-di-*O*-pentoside	593.00	447.07 $[M-H-pentoside-CH_3]^-$, 329.22 $[M-H-dipentoside]^-$, 263.04, 145.08, 163.07	+	+	+
66	8.407/18.508(L)	Luteolin-8-*C*-hexoside (orientin)	446.91	357.04 $[M-H-90]^-$, 327.06 $[M-H-120]^-$, 298.96, 284.69, 269.11, 297.12, 251.18, 253.22, 145.17	+***	+	+
67	8.767	Tricin	329.02	314.07 $[M-H-CH_3]^-$, 299.00 $[M-H-2CH_3]^-$, 269.05 $[M-H-2OCH_3]^-$, 283.12, 280.98, 271.01	−	+	+
68	9.702	Methyl-tricin *O*-rhamnoside-*O*-hexoside *O*-pentoside	785.09	639.24 $[M-H-146(Rha)]^-$, 491.16 $[M-H-132(pent)-162(hex)]^-$, 473.12 $[M-H-132(pent)-162(hex)-H_2O]^-$, 329.28 $[M-H-146(Rha)-162(hex)-132(pent)-CH_3]^-$	+	+	−
69	10.565	Methyl-tricin *O*-hexosyl pentoside	639.00	477.10 $[M-H-162(hex)]^-$, 329.17 $[M-H-)-162(hex)-132(pent)-CH_3]^-$	+	+	+
70	10.987	Tricin-*O*-rhamnoside-*O*-pentoside-*O*-hexosid	769.10	623.15 $[M-H-146(rham)]^-$, 475.08 $[M-H-162(hex)-132(pent)]^-$, 457.15 $[M-H-162(hex)-132(pent)-H_2O]^-$, 329.026 $[M-H-146(rham)-162(hex)-132(pent)]^-$	+	+	+
71	10.529	Tricin-*O*-rutinoside-*O*-hexoside-*O*-pentoside	931.06	785.18 $[M-H-146(rham)]^-$, 769.38 $[M-H-162(hex)]^-$, 637.06 $[M-H-162(hex)-132(pent)]^-$, 619.15 $[M-H-162(hex)-132(pent)-H_2O]^-$, 461.21 $[M-H-146(rham)-324(dihex)]^-$, 329.20 $[M-H-146(rham)-324(dihex)-132(pent)]^-$	+	+	−
72	11.66	Tetrahydroxyl dihydroflavone-*O*-rhamnoside	433.08	287.15 $[M-H-146(rham)]^-$, 163.09, 145.08, 165.05	+	−	−
Flavan-3-ol							
73	2.265	Catechin hexoside	1.13	405.03, 288.99 $[M-H-162(hex)]^-$, 245.05	−	−	+
74	2.743	Catechin	289.00	230.06, 227.01, 245.11, 221.07, 203.12, 188.07	−	−	+
75	2.959	(+)-Gallocatechin	305.00	261.00, 237.09, 221.05, 219.11, 179.05, 167.07, 147, 137.08	−	−	+

Table 1 (*Contd.*)

Peak no.	R_t (min)	Tentatively identified compounds	Mol. ion *m*/*z* ppm (−)	MS^2 major production	Organs		
					Leaf	Stem	Fruit
Flavanones							
76	3.504	Di-methoxy-naringenin	331.00	299.96 $[M\text{-}H\text{-}OCH_3]^-$, 270.99 $[M\text{-}H\text{-}2OCH_3]^-$, 271.89, 256, 243.06, 231.09, 227.15, 151.03, 119.06	−	+	−
77	5.451	Naringenin-8-*C*-hexoside	432.98	343.03 $[M\text{-}H\text{-}90]^-$, 313.07 $[M\text{-}H\text{-}120]^-$, 312.05, 311.03, 285.09, 255.13	+**	+	−
78	7.698	Naringenin-*O*-hexose *O*-rhamnoside	579.00	417.05 [M-H-162(hex)]$^-$, 271.14 [M-H-162(hex)-146(rham)]$^-$, 151.10	+	−	−
79	8.216	Naringenin-*O*-rhamnoside *O*-hexuornide	592.96	447.06 [M-H-146(rham)]$^-$, 417.04[M-H-176(glu)]$^-$	+	−	−
Aglycones							
80	3.760	Quercetin	300.95	255.12, 271.00, 163.06, 151.08, 227.02	−	+	−
81	3.880	Apigenine	268.96	241.08, 227.04, 225.01	+**	+**	−
82	5.308	Dihydroquercetin	303.15	285.01, 273.05, 256.92, 241.08, 217.07, 151.02, 153.07	−	+	−
83	7.942	Hesperetin	301.07	285.99 $[M\text{-}H\text{-}CH_3]^-$, 284.96, 283.04, 270.97, 255.14 $[M\text{-}H\text{-}OCH_3]^-$	−	+	−
84	8.108	Dihydroflavone, (di hydroluteolin)	287.16	285.19, 269.21, 241.72, 239.27	+	+	−
85	8.256	Pinocembrin	255.12	236.88 $[M\text{-}H\text{-}H_2O]^-$, 222.89, 213.07, 211.09	+	+	+
86	8.803	Kaempferol	285.01	267.02, 257.03, 241.01, 223.0, 229.07, 175.08, 151.08	+***	+	+**
87	8.975	Naringenin	271.00	151.06, 165.01, 177.02, 187.06, 145.06, 119.02	−	+	−
88	9.517	Luteoline	284.88	269.02, 267.01, 256.92, 241.08, 199.08, 133.08, 151.05, 175.10	+**	+	+
89	9.645	Acacetin (linarigenin)	283.17	268.04 $[M\text{-}H\text{-}CH_3]^-$, 265.03, 237.13	+**	+	+
90	10.087	Diosmetin	299.02	283.89 $[M\text{-}H\text{-}CH_3]^-$, 282.96, 254.97, 256.04	+	+	+
Dihydrochalcones							
91	4.996	Phloretin	272.99	241.02, 199.08, 227.04, 151.05, 152.04 139.09	−	+	−
92	5.142	Phloretin-*C*-hexsoside	434.89	417.00 $[M\text{-}H\text{-}H_2O]^-$, 389.17, 315.13 $[M\text{-}H\text{-}120]^-$	+	−	−
93	7.134	Phloretin-*O*-hexsoside (phlorizin) or (nothofagin)	435.01	389.12, 273.03 [M-H-162(hex)]$^-$	+	−	−
Lignans							
94	6.353	(−)-Syringaresinol-di-*O*-hexoside	741.04	417.02 [M-H-324(di-hex)]$^-$	−	+*	+*
95	6.356	(−)-Syringaresinol-*O*-hexoside	579.01	417.09 [M-H-162(hex)]$^-$, 402.14 $[M\text{-}H\text{-}162(hex)\text{-}CH_3]^-$	+*	+	+
96	6.708	Lariciresinol 4-*O*-exoside	521.10	359.13 [M-H-162(hex)]$^-$, 341.23 $[M\text{-}H\text{-}162(hex)\text{-}H_2O]^-$	+**	+	+
97	8.399	Secoisolariciresinol	361.11	346.15 $[M\text{-}H\text{-}CH_3]^-$, 315.12 $[M\text{-}H\text{-}CH_3\text{-}CH_2OH]^-$, 179.15 $[M\text{-}H\text{-}C_{10}H_{13}O_3]^-$	−	+	−
98	8.747	Pinoresinol	357.19	327.07 $[M\text{-}H\text{-}2CH_3]^-$, 309.16 $[M\text{-}H\text{-}2H_2O]^-$, 297.12 $[M\text{-}H\text{-}2OCH_3]^-$, 151.10, 136.18	+***	+	−

Table 1 (*Contd.*)

Peak no.	R_t (min)	Tentatively identified compounds	Mol. ion *m*/*z* ppm (−)	MS^2 major production	Organs		
					Leaf	Stem	Fruit
Triterbens							
99	10.18	Oleanolic acid-di-*O*-hexosyl ester	827.14	781.23 $[M-H-HCOOH]^-$, 619.24 $[M-H-162(hex)-HCOOH]^-$	−	+	+
100	11.76	Epimacherinic acid di-*O*-hexoside	811.19	765.20 $[M-H-HCOOH]^-$, 603.26 $[M-H-162(hex)-HCOOH]^-$	−	+	+
101	13.00	Hederagenin *O*-hexoside	679.21	633.22 $[M-H-HCOOH]^-$, 471.22 $[M-H-162(hex)-HCOOH]^-$	−	+	+
102	16.300	Oleanolic acid-*O*-hexosyl ester	663.15	455.19 $[M-H-162(hex)-HCOOH]^-$	−	+	+
103	23.402	Dihydro hederagenin *O*-hexoside	681.12	635.12 $[M-H-HCOOH]^-$	+	+	+
Fatty acids							
104	13.057	Hydroxy octadecadienoic acid	295.16	277.18, 259.19, 233.20, 183.19, 195.21, 155.18, 171.19, 139.19	+	+	+
105	13.753	Hydroxy octadecatrienoic acid	293.14	275.15, 264.98, 249.19, 236.02, 233.02, 221.17, 20.18, 205.15	+**	+	+
106	14.041	Dihydroxy-octadecadienoic acid	311.11	293.20, 267.09, 265.20, 239.12, 225.11, 171.24, 161.08	+	+	+
107	14.06	Oleic acid	281.18	263.65 $[M-H-H_2O]^-$, 237.32 $[M-H-CO_2]^-$, 183.24	+	−	−
108	14.495	Hydroxy octadecenoic acid	297.12	279.22, 251.24, 171.15	+*	+	−
109	14.558	Dihydroxy octadecatrienoic acid	309.10	291.12 $[M-H-H_2O]^-$, 265.20 $[M-H-CO_2]^-$, 263.32, 237.34, 205.10	+**	+	+
110	15.336	5,6,7-Triacetyl-2,3,5,6,7-pentahydroxyhexadecane-4,8,9-trione	473.20	429.23 $[M-H-CO_2]^-$, 411.73 $[M-H-CO_2-H_2O]^-$	+**	−	−
111	18.417	Octadecatrienoic acid	277.17	259.13, 233.19, 231.21, 205.09, 174.96	+**	+	+
112	19.42	Linolenic acid	277.17	233.41 $[M-H-COO]^-$, 141.21, 127.08	+	+	+
113	22.90	2,5,8,11,14,17,20-Heptaoxadocosan-22-ol	339.23	163.08 $[M-H-C_8H_{17}O_4^{\cdot}]^-$	+		+***
114	24.555	Palmitic acid	255.23	239.01, 236.99, 209.13, 210.97, 214.14	+	+	+
115	24.718	Octadecenoic acid	281.22	263.12 $[M-H-H_2O]^-$, 254.26 $[M-H-CO]^-$, 237.02 $[M-H-COO]^-$, 235.12 $[M-H-H_2O-CO]^-$, 219.01, 209.29, 181.10, 167.00	+	+**	+
116	27.905	Stearic acid	283.20	268.04, 265.03, 237.13, 198.11	+	+	+*

[a] The concentration of compounds in the extracts is denoted by *, **, and ***, where * signifies low concentration and *** denotes the highest.

2.7.2.2. Determination of minimum inhibitory concentration (MIC). The Minimum Inhibitory Concentration (MIC) was assessed to evaluate the antibacterial effectiveness of the plant extracts using the broth microdilution method, in line with the Clinical and Laboratory Standards Institute (CLSI) guidelines. Two-fold serial dilutions of the extracts were prepared in sterile nutrient broth, covering a concentration range from 250 mg mL^{-1} to 0.47 mg mL^{-1}, and were added to a 96-well microtiter plate. To each well, 100 μL of a bacterial suspension, adjusted to the 0.5 McFarland standard, was inoculated. The plates were then incubated at 37 °C for 24 hours, according to the specific growth conditions required for each bacterium. After the incubation period, the plates were examined for any visible bacterial growth. The MIC was determined as the lowest concentration of the extract that resulted in no visible microbial growth on the plate's surface.[19]

2.7.2.3 Statistical analysis. The inhibition zones were expressed as means ± standard deviation (SD). The data significance was assessed using analysis of variance (ANOVA), performed with the Microsoft Excel program. Differences in the data were considered significant at a 5% level.

3 Results and discussion

3.1. Analysis of qualitative data

We employed HPLC-ESI-MS/MS to characterize the phytochemical profile of the leaves, stems, and fruits of *P. aculeata* butanol extracts. This efficient and precise method for screening *P. aculeata* was enabled by the use of HPLC and the efficient extraction of the targeted plant parts. A negative ionization mode experiment was conducted to capture the diverse ionization and fragmentation characteristics of the polyphenolic metabolites in the BuOH extract of leaves, stems, and fruits. All substances were extracted and analyzed by considering solvent adducts and $[M - H]^-$ ions. The matched compounds were then characterized using established information, proposed fragmentation pathways, and additional data from the literature. This meticulous identification process revealed 116 distinct compounds were identified tentatively in the butanol extracts for the first time. The molecular networking facilitated the identification of 6 secondary metabolites. Flavonoids emerging as the predominant class of polyphenolics in *P. aculeata*. A diverse array of flavonoid derivatives, totaling approximately 71 compounds (19 flavonols, 31 flavones, 4 flavanones, 3 flavan-3ol, and 3 dihydrochalcones) were tentatively identified alongside other phytochemicals, including 19 phenolic acids, 5 lignans, 5 triterbens, 13 fatty acids and 2 organic acids. In addition to 6 unusual glycosides of flavones on the bases of GNPS libraries. The superimposed base peak intensity (BPI) chromatograms for the three extracts revealed a high degree of similarity between the leaves and stems, while the fruits extract showed significant variations, notably within the retention time (R_t) range of 11–21 min in the (−ve) negative mode (Fig. 2A–C).

3.2. The annotation of metabolites and molecular networking

3.2.1. Annotation of uncommon glycosylated flavones based on GNPS library. The molecular family of flavonoids, obtained from the molecular network in negative mode,

Table 2 Annotation of six uncommon di-*C*-glycosylated flavones on the bases of GNPS libraries, and their fragmentation pattern using HPLC-ESI-MS/MS in negative (−ve) ionization mode

Peak no.	R_t, (min)	Tentatively identified compounds	Mol. Ion *m/z* ppm (−)	MS^2 major production	Organs Leaf	Stem	Fruit
Uncommon glycosylated flavone derivatives							
A1	4.741	Chrysoeriol 6-*C*-pentoside 8-*C*-hexosyl-6‴ [(3-hydroxy-3-methylpentanedioic acid)]	736.92	592.96 [M-H-145($C_6H_9O_4^•$)]$^-$, 503 [M-H-145($C_6H_9O_4^•$)-90]$^-$, 473.04 [M-H-145($C_6H_9O_4^•$)-120]$^-$, 413.22 [M-H-145($C_6H_9O_4^•$)-120-60]$^-$, 383.09 [M-H-145($C_6H_9O_4^•$)-120-90]$^-$	+**	+	+
A2	3.139	Chrysoeriol 6,8-di-*C*-hexosyl-6‴ [(3-hydroxy-3-methylpentanedioic acid)]	766.96	676.97 [M-H-90]$^-$, 647.02 [M-H-120]$^-$, 503.06 [M-H-145($C_6H_9O_4^•$)-120]$^-$, 413.06 [M-H-145($C_6H_9O_4^•$)-120-90]$^-$, 383.13 [M-H-145($C_6H_9O_4^•$)-120-120]$^-$	+**	+**	+
A3	1.013	Chrysoeriol 6-*C*-rhamnoside-8-*C*-hexosyl-6‴ [(3-hydroxy-3-methylpentanedioic acid)]	751.00	607.06 [M-H-145($C_6H_9O_4^•$)]$^-$, 517.00 [M-H-145($C_6H_9O_4^•$)-90]$^-$, 487.05 [M-H-145($C_6H_9O_4^•$)-120]$^-$, 383.08 [M-H-145($C_6H_9O_4^•$)-90-104]$^-$	+**	−	+
A4	2.434	Chrysoeriol 6,8-di-*C*-hexosyl-6″,6‴-di[(3-hydroxy-3-methylpentanedioic acid)]	910.94	767.10 [M-H-145($C_6H_9O_4^•$)]$^-$, 677.04 [M-H-145($C_6H_9O_4^•$)-90]$^-$, 647.12 [M-H-145($C_6H_9O_4^•$)-120]$^-$, 413.15 [M-H-288($2C_6H_9O_4^•$)-90-1, 383.20 [M-H-288($2C_6H_9O_4^•$)-120-120]$^-$	+**	+	+
A5	4.963	Apigenin 6-*C*-pentoside 8-*C*-hexosyl 6‴[(3-hydroxy-3-methylpentanedioic acid)]	706.92	563.02 [M-H-145($C_6H_9O_4^•$)]$^-$, 472.94 [M-H-145($C_6H_9O_4^•$)-90]$^-$, 383.02 [M-H-145($C_6H_9O_4^•$)-120-60]$^-$, 353.5 [M-H-145($C_6H_9O_4^•$)-120-90]$^-$	+	+	+
A6	3.261	Apigenin 6,8-di-*C*-hexosyl-6″,6‴-di[(3-hydroxy-3-methylpentanedioic acid)]	880.58	737.01 [M-H-145($C_6H_9O_4^•$)]$^-$, 647.02 M-H-145($C_6H_9O_4^•$)-90]$^-$, 617.00 [M-H-145($C_6H_9O_4^•$)-120]$^-$, 473.07 [M-H-190($2C_6H_9O_4^•$)-120-]$^-$, 383.05 [M-H-190($2C_6H_9O_4^•$)-90]$^-$	+	+	+

revealed six rare flavone metabolites within cluster A (Fig. 4). These metabolites were annotated for the first time in *Parkinsonia* species and were generally distributed across the three investigated plant parts, with a higher abundance in the leaves. Most of them were chrysoeriol isomers (**A1–A4**) with deprotonated ions at *m*/*z* 736.92, 766.96, 751.00, and 910.94, respectively. Two apigenin isomers were appeared at *m*/*z* 706.92, and 880.58. Their identification was based on GNPS library matches and their characteristic fragmentation patterns (Table 2). Annotation was derived from the abundant fragments of deprotonated ions and their corresponding derivatives, primarily resulting from the loss of 145 Da ($C_6H_9O_4^{\bullet}$), corresponding to the cleavage of 3-hydroxy-3-methylpentanedioic acid. Additionally, neutral losses of $[M\text{-}H\text{-}90]^-$, $[M\text{-}H\text{-}120]^-$, $[M\text{-}H\text{-}60]^-$, and $[M\text{-}H\text{-}104]^-$ were observed, indicating sequential cleavage of hexose, pentose, and rhamnose units. Additional fragmentation generates ions compatible with [Ag + 113], [Ag + 83] indicative for di-*C*-glycosyl flavone fragmentation (ESI, Fig. S110–S115†). This pattern supports the existence of isomers of apigenin and chrysoeriol. Finally, based on this fragmentation behavior and GNPS library the compounds (**A1–A6**) were identified tentatively as chrysoeriol 6-*C*-pentoside 8-*C*-hexosyl-6‴[(3-hydroxy-3-methylpentanedioic acid)] (**A1**), chrysoeriol 6,8-di-*C*-hexosyl-6‴[(3-hydroxy-3-methylpentanedioic acid)] (**A2**), chrysoeriol 6-*C*-rhamnoside-8-*C*-hexosyl-6‴[(3-hydroxy-3-methylpentanedioic acid)] (**A3**), chrysoeriol 6,8-di-*C*-hexosyl-6″,6‴-di[(3-hydroxy-3-methylpentanedioic acid)] (**A4**), apigenin 6-*C*-pentoside 8-*C*-hexosyl 6‴[(3-hydroxy-3-methylpentanedioic acid)] (**A5**); and apigenin 6,8-di-*C*-hexosyl-6″,6‴-di[(3-hydroxy-3-methylpentanedioic acid)] (**A6**).

3.2.2. Determination and tentative identification of common phytochemical constituents

3.2.2.1. Phenolic acids. A total of 20 metabolites derived from phenolic acids and their glycosides were identified in butanol fractions and categorized into two main groups: hydroxybenzoic acids and hydroxycinnamic acids. Eight peaks corresponded to hydroxycinnamic acids and their glycosides, including cinnamic acid (**1**), ferulic acid (**8**), caffeic acid (**6**), caffeic acid hexoside (**7**), *O*-caffeoylquinic acid (**5**), coumaric acid (**18**), coumaric acid hexuornide (**14**), and coumaric acid di-*O*-hexuornide (**16**). Eleven ion intensity were attributed to hydroxybenzoic acids and their glycosides, which included *p*-hydroxybenzoic acid (**15**), *p*-hydroxybenzoic acid-4-*O*-hexoside (**20**), protocatechueic acid (**17**), protocatechuicaldehyde (**2**), vanillic acid (**13**), vanillic acid-*O*-hexoside (**12**), vanillic acid-*O*-rutinoside (**10**), gallic acid (**19**), methyl gallate (**22**), methyl gallate-*O*-hexoside (**9**), and hydroxy-anthranilic acid (**11**). Additionally, two organic acids were eluted first and detected: citric acid (**3**) and quinic acid (**4**). One phenolic compound, identified as 4-vinylphenol, was identified.

The analysis revealed that hydroxybenzoic acids were more abundant than hydroxycinnamic acids across all investigated plant parts (L, S, F). Their detailed MS/MS data, including how they fragmented and their elution times, are presented in (Table 1). All these phenolic acids showed strong peaks in mass spectrometry, either as negatively charged ions (M^- or $[M - H]^-$), representing their deprotonated molecules, or as smaller fragments (daughter ions). These fragments resulted from losing a carbon dioxide (CO_2) molecule; 44 amu or a water molecule (H_2O); 18 amu from the original ion (base ion). The consistent loss of 44 amu (carbon dioxide) is a key indicator used to identify phenolic acids.[20]

3.2.2.1.1. Free phenolic acids. Nine free phenolic acids (**1**, **6**, **8**, **18**, **17**, **19**, **11**, **15**, and **13**) were tentatively identified in the butanol extracts based on their mass-to-charge ratios (*m*/*z*), retention times (R_t), and characteristic fragmentation patterns consistent with previously reported data.[21] These phenolic compounds included cinnamic acid (*m*/*z* 146.90, R_t = 0.363), which exhibited fragment ions at *m*/*z* 102.95 $[M\text{-}H\text{-}COO]^-$ and 129.21 $[M\text{-}H\text{-}H_2O]^-$. Caffeic acid (*m*/*z* 179.08, R_t = 1.160) was characterized by fragment ions at *m*/*z* 161.06 $[M\text{-}H\text{-}H_2O]^-$ and 135.05 $[M\text{-}H\text{-}COO]^-$. Ferulic acid (*m*/*z* 192.99, R_t = 1.555) displayed fragment ions at *m*/*z* 174.98 $[M\text{-}H\text{-}H_2O]^-$, 156.94 $[M\text{-}H\text{-}2H_2O]^-$, and 149.04 $[M\text{-}H\text{-}COO]^-$. Coumaric acid (*m*/*z* 163.01, R_t = 2.983) was identified with fragment ions at *m*/*z* 144.92 $[M\text{-}H\text{-}H_2O]^-$ and 119.03 $[M\text{-}H\text{-}COO]^-$. Protocatechuic acid (*m*/*z* 153.00, R_t = 2.972) exhibited fragment ions at *m*/*z* 135.01 $[M\text{-}H\text{-}H_2O]^-$, 116.92 $[M\text{-}H\text{-}2H_2O]^-$, and 109.01 $[M\text{-}H\text{-}COO]^-$. Gallic acid (*m*/*z* 168.88, R_t = 3.064) was characterized by fragment ions at *m*/*z* 151.89, 150.92 $[M\text{-}H\text{-}H_2O]^-$, 132.94 $[M\text{-}H\text{-}2H_2O]^-$, and 125.05 $[M\text{-}H\text{-}COO]^-$. These phenolic acids were detected in all plant parts examined. Hydroxy-anthranilic acid (*m*/*z* 154.06, R_t = 1.872) was exclusively identified in the fruit butanol extract, with fragmentation patterns at *m*/*z* 135.96 $[M\text{-}H\text{-}H_2O]^-$, 117.95 $[M\text{-}H\text{-}2H_2O]^-$, and 110.05 $[M\text{-}H\text{-}COO]^-$. *p*-Hydroxybenzoic acid (*m*/*z* 137.00, R_t = 2.498) was detected solely in leaves extract, with fragment ions at *m*/*z* 118.99 $[M\text{-}H\text{-}H_2O]^-$ and 93.00 $[M\text{-}H\text{-}COO]^-$. Vanillic acid (*m*/*z* 167.01, R_t = 2.223) was found in both the stem and fruit extracts, exhibiting fragmentation patterns at *m*/*z* 149.03 $[M\text{-}H\text{-}H_2O]^-$, 123.02 $[M\text{-}H\text{-}COO]^-$, and 105.02 $[M\text{-}H\text{-}H_2O\text{–}COO]^-$, respectively.[22,23]

3.2.2.1.2. Phenolic acid glycosides. The main method for identifying and characterizing phenolic acid glycosides was to examine their fragmentation patterns, particularly the elimination of the glycosyl moiety and the carboxylic acid group. The presence or lack of the characteristic product ions produced by the carboxyl group's cleavage gave important information about where the sugar-linked sites were located in the glycoside molecules. With the use of this method, these compounds could be effectively differentiated and their structures clarified, underscoring the critical role that COO-group removal plays in their mass spectrometric analysis.[24]

In MS/MS analysis, five phytoconstituents identified as phenolic acid hexosides exhibited distinct fragmentation patterns, characterized by glycosidic bond cleavage and the absence of a typical CO_2 loss fragment. This behavior suggests that the glycosyl moiety is esterified to the phenolic molecule at the 1-*O*-position rather than being linked through an ether bond. For instance, MS/MS spectral data from the fruit revealed a key fragment at *m*/*z* 167.05 $[M\text{-}H\text{-}162(hex)]^-$ attributed to vanillic acid-*O*-hexoside (**12**). Similarly, the secondary ion detected in both the stem and fruit at *m*/*z* 167.05 $[M\text{-}H\text{-}308(rutinose)]^-$ was identified as vanillic acid-*O*-rutinoside (**10**).

An ion fragment at *m*/*z* 183.11 [M-H-162(hexose)]$^-$ was assigned to methyl gallate-*O*-hexoside was observed exclusively in the stem (**9**). Additionally, a daughter ion at *m*/*z* 163.07 [M-H-176(glucuronic acid)]$^-$/[M-H-352(di hexuornide)]$^-$ confirmed the presence of mono and di coumaric acid hexuornide (**14**, and **16**) in leaves and stems, respectively. The fragmentation pattern of peak **7**, highlighted by the production of key daughter ions at *m*/*z* 323.17 [M-H-H_2O]$^-$, *m*/*z* 297.19 [M-H-COO]$^-$, *m*/*z* 179.03 [M-H-162(hex)]$^-$, and *m*/*z* 135.05 [M-H-162(hex)-COO]$^-$, reveals a stepwise loss of COO, H_2O, and the sugar moiety. These distinctive ions, confirm that compound **7** as caffeic acid-*O*-hexoside detected in the extract's leaves, stems and fruits. Additionally, the data strongly indicate that the hexose is linked to caffeic acid through an ether bond rather than an ester bond. Similarly *p*-hydroxybenzoic acid hexosides (**15**) was tentatively identified in leaves butanol extract through its characteristic fragmentation profile. Key daughter ions observed at *m*/*z* 255.05 [M-H-COO]$^-$, *m*/*z* 237.03 [M-H-COO-H_2O]$^-$, *m*/*z* 137.02 [M-H-162(hex)]$^-$, and *m*/*z* 119.15 [M-H-162(hex)-H_2O]$^-$ suggest that the sugar moiety is linked to *p*-hydroxybenzoic acid through an ether bond rather than an ester bond.[25]

Peak **5**, the most abundant phenolic compound was identified across all examined plant parts, with its highest concentration observed in the fruits. The compound presented a parent ion at *m*/*z* 353.09 with a retention time of 1.127 min. Its fragmentation pattern revealed characteristic daughter ions at *m*/*z* 191.06, representing the loss of a caffeoyl group (162), and at *m*/*z* 179.03, corresponding to the loss of a quinate group (174). These findings strongly suggest that the compound is *O*-caffeoylquinic acid.

3.2.2.2. Flavonoids. The main aim of this study was to apply negative ionization mass spectrometry (MS) to identify flavonoids with notable biological activity and compare them to data from existing reports. The chemical structures of flavonoid derivatives were determined by examining their fragmentation patterns. Flavonoid glycosides tend to produce [M − H]$^-$ ions rather than [M + H]$^+$ ions. The MS/MS spectra revealed distinct fragment ions resulting from the retro-Diels–Alder fragmentation process, along with the loss of glycosyl groups in both (−ve) negative and (+ve) positive ion modes. Notable losses of ions included hexose (glucose or galactose), rhamnose, hexuronic acid (glucuronic acid), pentose (arabinose or xylose), and neohesperidoside (glucose + rhamnose), comparable to mass losses of 162, 146, 176, 132, and 308 amu, respectively, which were easily and specially apparent in the case of *O*-glycosides of flavonoids. Additionally, flavonoids showed a loss of 28 amu (CO), 18 amu (H_2O), and 15 amu (CH_3) confirming the presence of phenolic hydroxyl and CH_3 groups, aiding in the identification of different flavonoid subgroups.[26]

In compounds where two or more sugar molecules are attached to the same aglycone carbon, the ions generated from the cleavage of glycosidic bonds between the sugar units are typically weak. While the aglycone and glycane components are commonly identified. Determining the precise structure of flavonoid glycosides remains challenging. This difficulty arises because the identity of the monosaccharides and their specific attachment sites cannot always be established using LC-MS alone. Ultimately, the structures of these compounds were confirmed through comparison with previously reported data in the literature.[27]

LC-MS/MS analysis of *C*-glycosides revealed a key product ions [M-H-90($C_3H_6O_3$)]$^-$ & [M-H-120($C_4H_8O_4$)]$^-$ characteristic for hexose cleavage and [M-H-90]$^-$ &[M-H-60]$^-$ characteristic for pentose cleavage, as well as the absence of the [M-H-hexose]$^-$ and [M-H-pentose]$^-$ ions for ether-linked glycosides. In contrast to *O*-glycosides, which are easily loss the sugar moiety, due to the ease with which oxygen (O) becomes ionized and the fact that the O–C bond is more susceptible to cleavage than the C–C bond under MS analysis conditions.[28,29]

The *C*-glycosylated flavonoids prefer breaking apart on the glycosidic moiety, and the resulting ions are aglycones with connected sugar moieties. We identify the nature of the aglycone, whether it is a monoglycoside or a diglycoside, through their characteristic ions, as it loses [aglycone + 41]; [aglycone + 71] in mono-*C* and [aglycone + 83]; [Ag + 113] in di-*C*-glycoside. The majority of *C*-glycosides have sugars attached at the C-6 and/or C-8 positions, so it was important to distinguish between 6-*C* and 8-*C* glycosylated flavones and determine the type of sugar substituted at the *C*-6 and *C*-8 positions.[30,31]

In 6-*C*-glycosylated flavonoids, there is a clear loss of H_2O in the deprotonated ion compared to 8-*C*-glycosylated flavonoids. In 6-*C*-glycosylated flavonoids H_2O can easily lose between the OH- group at the 2″-position of the sugar and its counterpart at the 5- or 7-OH position of the aglycone. However, the mechanism of H_2O loss in 8-*C*-glycosyl flavonoids is limited to the 7-OH group and is inhibited by hydrogen bonding between the 7-OH group of the aglycone and the sugar atom. The relative ion intensities of [M-H-90] in 6-*C*-isomers are higher than in 8-*C*-isomers (ESI, Fig. S108), which is another notable distinction between the two isomers. Two characteristics of 2″-*O*-glycosyl-*C*-glycosyl derivatives are the presence of an abundant ion [M-H-132/-146/-162]$^-$, preferential fragmentation that results in a relevant [M-H-18]$^-$ fragment; and the *O*-glycosylation at position 6″ of the sugar moiety from *C*-glycosylation, which causes loss [M-H-162-120]$^-$ and [M-H-162-90]$^-$ from *C*-glycosylation.[30,32]

3.2.2.2.1. Flavonols. ***Kaempferol-based derivatives***: Several kaempferol derivatives, peaks (**23–25**, **33**, **35**, and **40**) were detected in the butanol extract of leaves, stems, and fruits. The majority of these compounds were found to be glycosides with a single sugar moiety. Kaempferol was identified in both *C*-glycosylated and *O*-glycosylated forms, distinguished by their characteristic MSn fragmentation patterns. The *C*-glycosylated forms exhibit a carbon–carbon bond that is resistant to cleavage, with fragmentation primarily occurring at the sugar bonds. In contrast, *O*-glycosylated kaempferol readily loses its sugar moiety through neutral loss.

The leaves extract was the only source of one such *O*-glycosylated kaempferol, referred to as compound **23**. This compound exhibited an [M − H]$^-$ ion at *m*/*z* 430.93, and its MS/MS spectrum revealed a fragment ion at *m*/*z* 285.12, indicating a neutral loss of 146 amu, corresponding to rhamnoside. Further fragmentation of the *m*/*z* 285 ion produced

characteristic kaempferol fragments at *m*/*z* 241.11 and 223.08. Based on this data, compound **23** (ESI, Fig. S35) was identified as kaempferol-*O*-rhamnoside.[33] The *C*-glycosylated kaempferol derivatives were identified in both leaves and stems. Compounds **24** and **33** exhibited the same $[M-H]^-$ ions at *m*/*z* 446.90, while compound **25** showed a $[M-H]^-$ ion at *m*/*z* 448.93, corresponding to its dihydro form. The MS/MS analysis revealed fragmentation patterns characteristic of mono-*C*-glycosides, with fragment ions at *m*/*z* 357, 327, 359, and 329, resulting from neutral losses of 120 and 90 amu, respectively. These neutral losses indicate the presence of a hexose moiety. Given that the 6-*C*-hexoside elutes before the 8-*C*-hexoside isomer, compounds **24**, **33**, and **25** were identified as kaempferol-6-*C*-hexoside, kaempferol-8-*C*-hexoside, and dihydrokaempferol-6-*C*-hexoside, respectively.[4]

Two isomers of kaempferol were identified in both leaves and fruits extract, both yielding the same $[M-H]^-$ ions at *m*/*z* 298.96. The fragmentation pattern observed was typical of methoxylated flavonoids, with a key fragment at *m*/*z* 284.00 corresponding to $[M\text{-}H\text{-}CH_3]^-$. This fragmentation profile is consistent with that of isokaempferide (**35**) and rhamnocitrin (**40**).[34]

Quercetin-based derivatives: A total of 11 quercetin derivatives were detected in the butanol extracts and tentatively identified as follows: peak **26** (R_t = 5.55) presented a quasi-molecular ion peak at *m*/*z* 608.95 and a fragmentation pattern corresponding to a disaccharide residue consisting of rhamnose and hexose; the fragment ion at *m*/*z* 300.12[M-H-308(rutinose)]$^\bullet$ is more intense than the ion at *m*/*z* 301.14[M-H-308(rutinose)]$^-$, suggesting that a disaccharide is attached at the 3-OH position (ESI, Fig. S90). Quercetin-di-*O*-glycosides (R_t = 8.39) appeared as a base peak at *m*/*z* 623.05, accompanied by daughter ions at *m*/*z* 477.10 and 447.08. The ion at *m*/*z* 477.10, resulting from the loss of a rhamnoside unit at first [M-H-146(rham)]$^-$, suggests substitution at position 7. This is further supported by the identification of quercetin 7-*O*-rhamnoside (*m*/*z* 447.10) and previous studies indicating that the initial fragmentation of flavonol compounds typically involves cleavage of the *O*-glycosidic bond at position 7, followed by the breakdown of the moiety linked to position 3.[35] Additionally, the appearance of the ion at *m*/*z* 447.08 [M-H-176(gluc)]$^-$ confirms the presence of a hexuornide unit at position 3. Based on this evidence, compound **37** is tentatively identified as quercetin 7-*O*-rhamnoside-3-*O*-hexuornide, found in both leaves and fruits.

Four isomers of dimethylquercetin glycosides were tentatively identified, presenting $[M-H]^-$ ions at *m*/*z* (463.10, R_t = 6.60 min)/(490.95, R_t = 7.34 min)/(653.05, R_t = 6.75 min)/(622.95, R_t = 6.09 min) in the mass spectrum. The MS^2 spectra revealed fragment ions characteristic of *O*-glycosides. Among these, the ion at *m*/*z* 331.12[M-H-132]$^-$, and 301.06[M-H-132-2CH_3]$^-$, correspond to dimethylquercetin-7-*O*-pentoside (**31**) which was specifically detected in leaves. The ions recognized in the leaves, stems, and fruits at *m*/*z* 329.05 [M-H-162(hex)], 314.13 [M-H-162(hex)-CH_3]$^-$, 299.03 [M-H-162(hex)-2CH_3]$^-$, prove the presence of dimethylquercetin-*O*-hexoside (**36**). Additionally, the appearance of daughter ions at *m*/*z* 491.09 [M-H-162(hex)]$^-$ and 329.17 [M-H-324(dihex)]$^-$ suggest the presence of two hexose units attached to the same hydroxyl group (OH) on the aglycone. Based on the evidence presented, metabolite **34** has been identified as dimethylquercetin di-*O*-hexoside.[36]

The detection of fragments associated with both *O*- and *C*-glycosylation patterns in leaves sample at *m*/*z* 491.11 [M-H-132]$^-$, 341.08 [M-H-132-2CH_3-120]$^-$, confirm the presence of a dimethylquercetin di-glycoside structure (*m*/*z* = 653.05, R_t = 6.75) comprising pentose and hexose units. The sequential loss of a pentose unit followed by the cleavage of a hexose unit indicates that the pentoside occupies a terminal position, while the hexoside is directly linked to the aglycone, forming a pentosyl–hexoside arrangement. Additionally, the ion resulting from a 120 amu loss after the elimination of both the pentose and dimethyl groups supports the presence of *O*-pentosyl-*C*-hexoside moieties. The absence of fragment ions corresponding to the loss of 90 amu rules out attachment of the *C*-hexoside at the 6-*C* position and confirms its linkage at the 8-*C* position of the aglycone. Based on this evidence, the metabolite **28** has been identified as dimethylquercetin 7-*O*-pentoside-8-*C*-hexoside.

The analysis identified two mono *C*-glycosidic derivatives of quercetin in both leaves and stems extract. Metabolite **32** exhibited a base peak at *m*/*z* 463.10, with prominent MS fragments at *m*/*z* 372.87 [M-H-90]$^-$ and 342.97 [M-H-120]$^-$. Notably, the absence of a fragment at *m*/*z* 355, which corresponds to the loss of a water molecule (18 amu) in addition to 90 amu [M-H-90-H_2O]$^-$, was critical in the structural elucidation. According to established guidelines for identifying isomeric 8-*C*-glycoside flavonoids, this compound was conclusively identified as quercetin-8-*C*-hexoside. Compound **29** (*m*/*z* 477.06, R_t = 6.31) displayed a similar fragmentation pattern consistent with 8-*C*-hexosides, producing fragments at *m*/*z* 386.93 [M-H-90]$^-$, 356.94 [M-H-120]$^-$and 329.01 [Ag + 14]. Based on this fragmentation behavior, compound **29** was assigned as isorhamnetin-8-*C*-hexoside.[37].

Peak **30**, found only in leaves extract, presented a molecular ion peak at *m*/*z* 623.3. In MS^2, it suffered neutral losses of 132 amu (pentoside) and 176 amu (hexuornide), resulting in the aglycone ion at *m*/*z* 315.11. The aglycone was assigned as isorhamnetin, based on the loss of [M-H-132-176]$^-$ from the base peak at *m*/*z* 623.3. The discovery of a daughter ion at *m*/*z* 491.06 and a fragment at *m*/*z* 315.11 provided further structural insight. These fragments suggest that the pentoside occupies the terminal position in the diglycoside moiety, while the hexuornide is directly attached to the aglycone forming a pentosyl–hexuornide arrangement. Based on this information, the compound was proposed to be isorhamnetin-*O*-pentosyl hexuornide.

Myrecetin-based derivatives: Two syringetin analogs labeled as peaks **27** and **41**, were tentatively assigned for the first in *P. aculeata* using total ion chromatography (TIC) and base peak chromatography (BPC). These metabolites exhibited distinct elution times of 5.96 min and 10.53 min with precursor ion mass-to-charge ratios (*m*/*z*) of 683.01 and 639.08, respectively. Metabolite **27** was observed exclusively in the stem and presented a pseudomolecular ion peak at *m*/*z* 683.01. Its

fragmentation pattern revealed daughter ions at *m*/*z* 521.04 [M-H-162(hex)]$^-$ and 345.23 [M-H-162(hex)-176(gluc)]$^-$. These results indicate that the hexoside is located at the end of the diglycoside moiety, whereas the hexuornide is directly connected to the aglycone. This structural configuration corresponds to a hexosyl-hexuornide arrangement, leading to the tentative identification of this compound as syringetin *O*-hexosyl hexuornic acid. Metabolite **41** was detected across all examined plant parts and exhibited a pseudomolecular ion peak at *m*/*z* 639.08. The fragmentation pattern generated daughter ions at *m*/*z* 477.14 [M-H-162(hex)]$^-$ and *m*/*z* 345.15 [M-H-162(hex)-132(pent)]$^-$, indicating a direct relationship between the hexosyl–pentoside disaccharide structure and the aglycone. Based on this evidence, compound **41** was identified as syringetin-*O*-hexosyl pentoside.

3.2.2.2.2. Flavones. ***Apigenin-based derivatives***: Five apigenin derivatives (compounds **44**, **50**, **51**, **53** and **54**) were identified in the butanol extract for the first time and distributed in all examined parts of *P. aculeate*. They confirmed by their fragmentation pattern and GNPS library (Fig. 3).

Mono-*C*-glycosylated derivatives of apigenin observed in cluster B exhibited key fragment ions at [M-H-90]$^-$ and [M-H-120]$^-$, indicating the presence of 6-*C*- or 8-*C*-linked hexosides. The prominent ion at *m*/*z* 311.07 [M-H-120]$^-$ alongside a weaker fragment at *m*/*z* 341.04 [M-H-90]$^-$ suggests that the hexose is attached at the 8-*C* position. Consequently, compound **51** was tentatively identified as apigenin-8-*C*-hexoside. In contrast, the strong ion at *m*/*z* 341.03 [M-H-90]$^-$ with high intensity, followed by an abundant ion resulting from the loss of [M-H-90-H_2O]$^-$, indicates that the hexose is linked at the 6-*C* position. Thus, compound **54** was proposed to be apigenin-6-*C*-hexoside.

For di-*C*-glycosides observed in cluster B, the characteristic neutral losses produce fragment ions at *m*/*z* 503.11 [M-H-90]$^-$, 473.10 [M-H-120]$^-$, and 413.20 ([M-H-180]$^-$), corresponding to sequential losses of hexose units. Additional fragmentation generates an ion at *m*/*z* 383.20 [M-H-90-120]$^-$, which is compatible with [Ag + 113] and indicative of di-*C*-glycosyl flavone fragmentation. This pattern supports the existence of apigenin as the aglycone (MW = 270). Based on this fragmentation behavior and GNPS library (Fig. 4), compound **44** was identified as an isomer of apigenin 6, 8-di-*C*-hexoside (vicenin-2).

Furthermore, the additional loss of an *O*-rhamnoside moiety, producing fragments at *m*/*z* 323.20 [M-H-90-146(rham)-18(H_2O)]$^-$ and *m*/*z* 293.02 [M-H-120-146(rham)-H_2O(18)]$^-$, confirmed the triglycoside structure of apigenin and identified metabolite **53** as isovitexin *O*-rhamnoside.[38] The apigenin aglycone (**81**) was tentatively identified in leaves and stems based on the precursor ion observed at *m*/*z* 268.96.

A minor peak was detected exclusively in the stem at *m*/*z* 445.03, with a retention time (R_t) of 4.512 min. Fragmentation analysis presented an ion at *m*/*z* 283.06 [M-H-162(hex)]$^-$, characteristic of the acacetin aglycone (**89**), indicating the loss of a mono-hexose unit. This evidence led to the identification of the compound **50** as acacetin-*O*-hexoside.

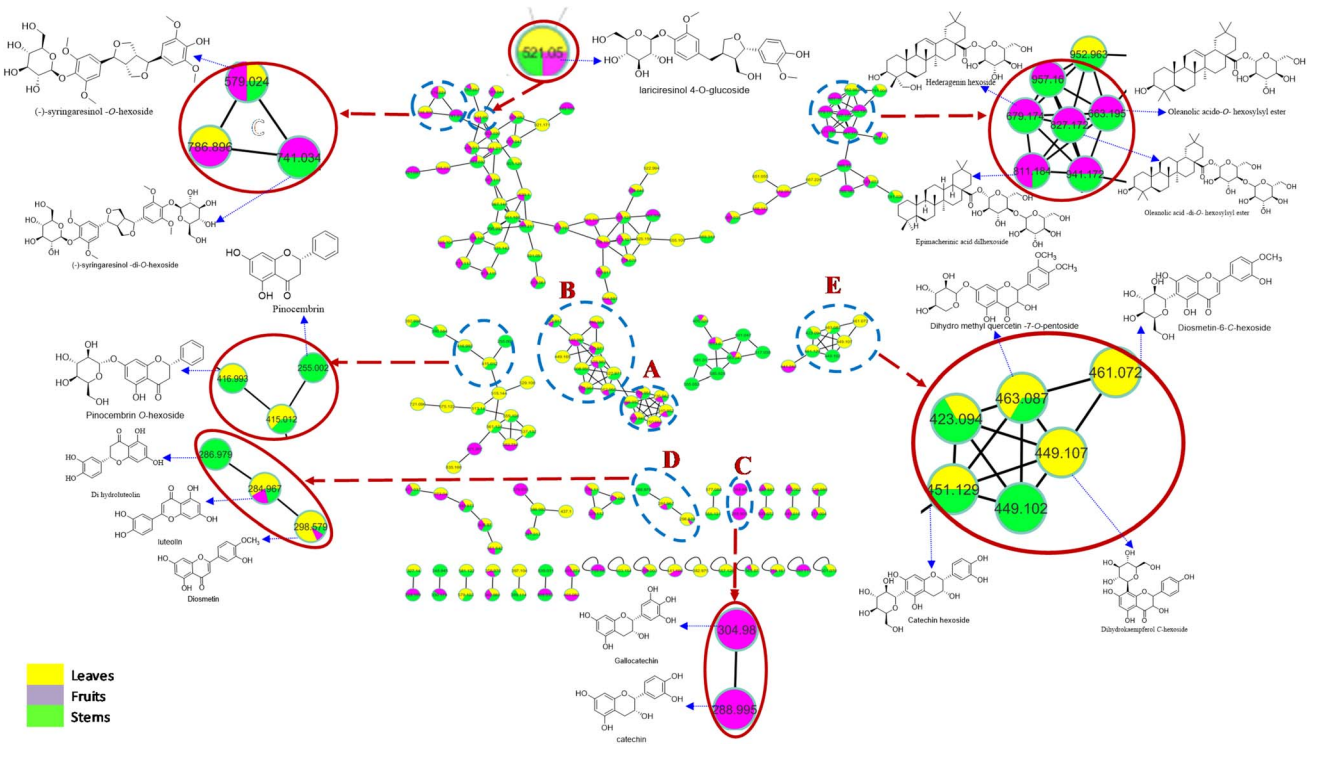

Fig. 3 Comprehensive molecular networking generated from MS/MS data in negative ionization mode for the butanol extracts of *P. aculeata* leaves, stems, and fruits. The nodes are annotated with parent masses and visualized as pie charts, where the colors yellow, purple, and green represent the relative distribution of precursor ion intensity across the respective plant parts. Clusters A–E contains nodes that correspond to matches in the GNPS spectral libraries.

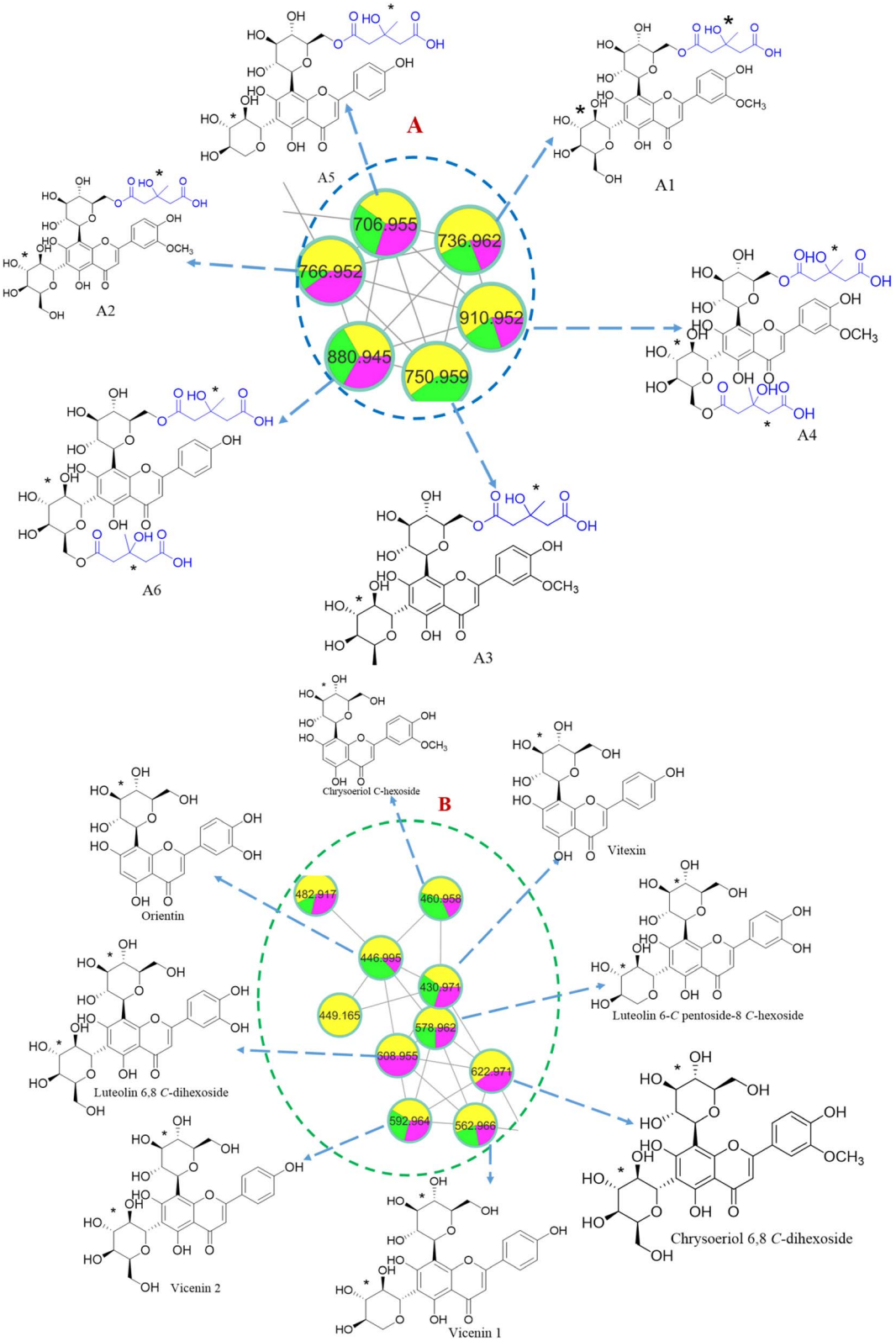

Fig. 4 Comprehensive molecular network constructed from MS/MS data in negative ionization mode for butanol extracts of *P. aculeata* leaves, stems, and fruits. Cluster A represents uncommon glycosylated flavones, while cluster B consists of flavones identified for the first time in the stems and fruits. *Note: substitution positions may vary.

Luteolin-based derivatives: The total ion current (TIC) and base peak chromatograms (BPC) presented 8 luteolin mono-and di-hexosides; peaks **61**, **66**, **42**, **46**, **49**, **52**, **49**, and **59** with molecular ions matching the following *m*/*z* values and retention times (R_t): 446.90 (R_t = 5.818), 446.91 (R_t = 8.407), 608.95 (R_t = 1.529), 578.93 (R_t = 3.01), 592.99 (R_t = 3.809), 739.00 (R_t = 5.428), 607.00 (R_t = 3.767), and 593.06 (R_t = 6.603), respectively. The tentative identification of these metabolites can be confirmed as follows.

A pair of mono-*C*-hexoside flavonoids with identical deprotonated precursor ions $[M-H]^-$ at *m*/*z* 446.90 were detected, expressing different retention times (R_t): 5.518 and 8.407 min. The MS^2 fragmentation gave ions at *m*/*z* 357.06/357.04, 327.11/327.06, and 298.96/299.10, resembling the fragmentation pattern characteristic of luteolin *C*-hexoside. The differentiation between 6-*C*- and 8-*C*-glycosidic linkages was determined based on diagnostic MS^2 and MS^3 fragment ions. Notably, the ions at *m*/*z* 428.95 $[M-H-18(H_2O)]^-$ and 410.96 $[M-H-36(2H_2O)]^-$, along with the MS^3 ion at *m*/*z* 309, were characteristic of isoorientin(luteolin 6-*C*-hexoside) and were absent in orientin(luteolin 8-*C*-hexoside). The 6-*C*-glycoside was characterized by a prominent base peak at *m*/*z* 357.06, whereas the 8-*C*-glycoside displayed a base peak at *m*/*z* 327.06. Peak **61** presented ions at *m*/*z* 357.06 $[M-H-90]^-$, 327.11 $[M-H-90-18]^-$, 339 $[M-H-120]^-$, $[aglycone + 71]^-$, and $[aglycone + 41]^-$. These represent a typical MS^2 fragmentation pattern of mono 6-*C*-glycosylated flavones.[39,40] Based on the above findings, peaks **61** and **66** were detected in all analyzed plant parts and recognized as luteolin 6-*C*-hexoside and luteolin 8-*C*-hexoside, respectively. These compounds has been reported earlier in *Parkinsonia* species.[11] Two analogs of di-*C*-glycosides of luteolin were detected in *P. aculeata* for the first time. They gave deprotonated precursor ions $[M-H]^-$ at *m*/*z* 608.95 and 578.93. The MS/MS spectral analysis of peak **42** presented typical fragmentation behavior for symmetrical di-*C*-glycosides. The observed daughter ions included $[M-H-18(H_2O)]^-$, $[M-H-90]^-$, [M-H-120], $[M-H-180]^-$, $[M-H-210(90+120)]^-$, $[M-H-240(120+120)]^-$, $[Ag+113]^-$, and $[Ag+83]^-$, respectively. Key fragment ions were detected at *m*/*z* 399.10, 369.05, and 428.91 $[M-H-180(90+90)]^-$. Based on these findings, compound **42** was preliminarily identified in both leaves and stems as luteolin 6, 8-di-*C*-hexoside. The typical fragmentation pattern of di-*C*-asymmetric glycosyl of luteolin (hexose and pentose) was observed at *m*/*z* 560.92 $[M-H-18]^-$, 518.91 $[M-H-60]^-$, 488.96 $[M-H-90]^-$, 458.92 $[M-H-120]^-$, and 428.97 $[M-H-150]^-$. To identify the aglycone, the fragments at *m*/*z* 399.09 [Ag + 113] and 369.06 [Ag + 83] were examined, indicating a molecular weight of 285 amu for the aglycone. This mass likely corresponds to luteolin (**88**). The compound (**46**) was subsequently identified in both leaves and stems as luteolin-*C*-hexoside-*C*-pentoside.[41]

Two di-*O*-glycosylated flavones were found for the first time in stem. They produced different precursor ions at *m*/*z* (607.00, 593.06) and identical daughter ion at *m*/*z* 285.00, indicating the neutral loss of their respective diglycoside moieties. For metabolite **48**, a fragment loss of 322 amu was observed, which corresponds to the combined neutral loss of 146 amu from rhamnose (rham) and 176 amu from hexuornic acid (gluc). This confirmed the structure of metabolite **48** as luteolin-*O*-rhamnoside-*O*-hexuornide, representing its first reported occurrence in *P. aculeata*. Similarly, for metabolite **59**, a neutral loss of 308 amu was detected, representing the combined loss of 162 amu from hexose (Hex) and 146 amu from rhamnose (rham). This established the identity of metabolite **59** as luteolin7-*O*-rutinoside, previously reported in the aqueous fraction of *P. aculeata.*[10]

Compound **49**, a highly abundant metabolite detected exclusively in stems, exhibited a precursor ion at *m*/*z* 592.99 and eluted at 3.909 min, along with five key fragment ions. The first fragment appeared at *m*/*z* 502.99 $[M-H-90]^-$, while the second was observed at *m*/*z* 473.02 $[M-H-120]^-$. Additional fragments presented characteristic patterns of a *C*-/*O*-dihexoside structure, including *m*/*z* 357.18 $[M-H-90-146(rham)]^-$ and *m*/*z* 327.18 $[M-H-120-146(rham)]^-$. These fragments correspond to (Ag + 71) and (Ag + 41), respectively, confirming the presence of *C*- and *O*-glycosidic moieties: a hexose linked *via* a *C*-glycosidic bond and a rhamnose linked *via* an *O*-glycosidic bond. Based on these data, metabolite **49** was identified as luteolin 8-*C*-hexoside *O*-rhamnoside. Peak **52** (R_t = 5.428 min) exhibited a base peak observed exclusively in leaves at *m*/*z* 739.00. This corresponds to the molecular ion of peak **49** (*m*/*z* 593) with an additional 146 mass units, attributed to a rhamnosyl moiety. The MS fragmentation pattern strongly suggests the presence of luteolin triglycosides. Two key fragment ions appeared at *m*/*z* 327.42 $[M-H-292(dirham)-120]^-$ and 285.01$[M-H-292(di-rham)-162(hex)]^-$ proving compound **52** as luteolin 8-*C*-hexoside di-*O*-rhamnoside, representing its first reported occurrence in *P. aculeate*.

Tricin-based derivatives: The butanol extracts analysis detected 6 tricin isomers, which were separated into two structural groups: methylated and non-methylated tricin glycosides. Mono-, di-, tri-, and tetra-*O*-glycosides were tentatively identified within both groups, based on characteristic mass losses associated with the fragmentation patterns of *O*-glycosides. The MS analysis of all isomers consistently generated fragment ions at *m*/*z* 329, suggesting the presence of a tricin aglycone (**67**), the loss of a glucuronic acid unit (176 amu) was a hallmark feature in MS/MS analysis of tricin-*O*-hexuornide (**63**), which was initially detected in both the stem and fruit and unreported in *P. aculeata*. Metabolite **65** presented a base ion signal at *m*/*z* (593.00, R_t = 8.207 min) and key ion fragments at *m*/*z* 447.07 $[M-H-pentoside-CH_3]^-$, and 329.22 $[M-H-dipentoside]^-$, leading to its tentative identification as tricin-di-*O*-pentoside.[10] A tri-glycoside compound (**70**) was tentatively assigned in leaves, stems, and fruits, and not recognized before in *P. aculeate.* It was proposed as tricin-*O*-rutinoside-*O*-pentoside. This proposal was based on prominent daughter ions resulting from the loss of rutinosyl pentoside structure (trisaccharide) with key fragments observed at *m*/*z* 623.15 $[M-H-146(rham)]^-$, 475.08 $[M-H-162(hex)-132(pent)]^-$, 329.026 $[M-H-146(rham)-162(hex)-132(pent)]^-$. The *tet*-*O*-glycoside tricin (**71**) gave base peak at *m*/*z* 931.06, similar to compound **70** but with the addition of a hexose unit. Key ions included *m*/*z* 785.18 $[M-H-146(rham)]^-$, 769.38 $[M-H-162(hex)]^-$, 637.06 $[M-H-162(hex)-132(pent)]^-$, 619.15 $[M-H-162(hex)-132(pent)-H_2O]^-$, and 461.21 $[M-H-146(rham)-324(dihex)]^-$. Based on these observations, metabolite **71** was detected in leaves and stems as tricin-*O*-

rutinoside-*O*-hexoside-*O*-pentoside, not mentioned before in *P. aculeate*.

Peak **68** (*m*/*z* 639.00, $R_t = 10.565$ min), discovered for the first time in *P. aculeate*. In our research it detected in both leaves and stems samples, and tentatively identified as a methylated tricin *O*-glycoside. Fragmentation analysis revealed the loss of a hexose moiety, producing a daughter ion at *m*/*z* 477.10 $[M\text{-}H\text{-}162(hexose)]^-$. Further fragmentation generated an ion at *m*/*z* 329.17 $[M\text{-}H\text{-}162(hexose)\text{-}132(pentose)\text{-}CH_3]^-$, indicating the sequential loss of a pentose and a methyl group. These results strongly suggest the presence of a methylated tricin di-*O*-glycoside. The absence of a daughter ion at *m*/*z* 507 confirmed that both glycosides are attached at the same position on the aglycone, forming a diglycoside structure. Additionally, the presence of a daughter ion at *m*/*z* 447 (loss of hexose), followed by *m*/*z* 329 (loss of pentose), indicates that the hexose moiety is in a terminal position, while the pentose is directly linked to the aglycone. This arrangement corresponds to a hexosyl–pentoside linkage.[42] Based on these findings, compound **68** was tentatively identified as methyl-tricin *O*-hexosyl pentoside. Compound **69** (*m*/*z* 785.09, $R_t = 9.702$ min) is structurally similar to compound **70**, distinguished by the addition of a methyl group. Key ions detected include *m*/*z* 639.24 $[M\text{-}H\text{-}146(rha)]^-$, 491.16 $[M\text{-}H\text{-}132(pent)\text{-}162(hex)]^-$, 473.12 $[M\text{-}H\text{-}132(pent)\text{-}162(hex)\text{-}H_2O]^-$, and 329.28 $[M\text{-}H\text{-}146(rha)\text{-}162(hex)\text{-}132(pent)\text{-}CH_3]^-$. These findings indicate that metabolite **69** is present in the leaves and stems as methyl-tricin *O*-rhamnoside-*O*-hexoside-*O*-pentoside, and was initially detected in *P. aculeate*.

Diosmetin-based derivatives: Two diosmetin mono-*C*-hexosides with identical deprotonated precursor ions $[M\text{–}H]^-$ at *m*/*z* 460.99 were identified, exhibiting distinct time elution (R_t) of 6.297 and 6.417 min. MS^2 fragmentation presented ions at *m*/*z* 371.01 $[M\text{-}H\text{-}90]^-$; [Ag + 41] and 341.04 $[M\text{-}H\text{-}120]^-$; [Ag + 71], consistent with the characteristic fragmentation patterns of diosmetin 6-*C*- and 8-*C*-hexoside. Differentiation between the two compounds was achieved through diagnostic MS^2 and MS^3 fragment ions. Specifically, the ion at *m*/*z* 353.08 $[M\text{-}H\text{-}90\text{-}18(H_2O)]^-$, accompanied by MS^3 ion at *m*/*z* 309, was a unique marker for diosmetin-6-*C*-hexoside (**56**) and was absent in diosmetin-8-*C*-hexoside (**58**). Diosmetin-6-*C*-hexoside was exclusively identified in leaves, whereas diosmetin-8-*C*-hexoside was found across all examined plant parts.[43] Similarly, peak **45**, characterized by the additional loss of a *C*-pentoside $[M\text{-}H\text{-}60]^-$ at *m*/*z* 533.04 and $[M\text{-}H\text{-}90]^-$ at *m*/*z* 503.00, alongside key ions characteristic of di-*C*-glycosides at *m*/*z* 383 [Ag + 83] and *m*/*z* 413.01 [Ag + 113]. The observed molecular weight of 299 amu corresponds to the aglycone diosmetin (**90**). The fragmentation pattern includes a daughter ion resulting from the loss of a water molecule at *m*/*z* 575.03 $[M\text{-}H\text{-}18(H_2O)]^-$, followed by ions at *m*/*z* 533.04 $[M\text{-}H\text{-}60]^-$ and *m*/*z* 503 $[M\text{-}H\text{-}90]^-$. These characteristic fragments confirm the presence of a pentoside attached at the 6-*C* position of the aglycone and a hexoside at the 8-*C* position. Based on this evidence, compound **45** was identified in leaves, stems, and fruits as diosmetin 8-*C*-hexoside 6-*C*-pentoside.[44]

The detection of a daughter ion at *m*/*z* 298.96 $[M\text{-}H\text{-}162(hex)]^-$ indicates that peak **62** corresponds to diosmetin-*O*-hexoside. Additionally, the presence of a daughter ion at *m*/*z* 475.05, representing the loss of a pentose, followed by an ion at *m*/*z* 298.99, signifying the loss of a hexuornide, provides insights into the molecule's structural arrangement. Specifically, the pentose moiety occupies the terminal position, while the hexuornide group is directly attached to the aglycone, consistent with a pentosyl–hexuornide linkage. Based on this evidence, metabolite **60** was tentatively identified as diosmetin *O*-pentosyl hexuornide, detected for the first time exclusively in the fruit extract.

Two isomers of chrysoeriol were identified in *P. aculeata* and tentatively assigned based on their precursor ions and retention times (R_t). The first isomer, a symmetrical di-*C*-glycoside, was detected at *m*/*z* 623.01 with a retention time of 2.291 min, while the second isomer, an asymmetrical *C*-/*O*-glycoside, appeared at *m*/*z* 606.98 with a retention time of 5.670 min. The symmetrical di-*C*-glycoside isomer exhibited characteristic fragment ions that correspond to the stepwise loss of two hexose residues. These included *m*/*z* 533.06 $[M\text{-}H\text{-}90]^-$, *m*/*z* 503.05 $[M\text{-}H\text{-}120]^-$, and *m*/*z* 383.04 $[M\text{-}H\text{-}240]^-$, along with fragments at *m*/*z* 413.05 $[M\text{-}H\text{-}120\text{-}90]^-$, corresponding to [Ag + 83], and *m*/*z* 533.06, corresponding to [Ag + 113]. Based on this fragmentation pattern, compound **43** was tentatively identified in the leaves and stems as chrysoeriol 6,8-di-*C*-hexoside. The asymmetrical *C*-/*O*-glycosides were identified as the predominant isomers in leaves, producing daughter ions characteristic of *C*- and *O*-linked hexoses. These ions were detected at *m*/*z* 486.96 $[M\text{-}H\text{-}120]^-$, 341.16 $[M\text{-}H\text{-}120\text{-}146(rham)]^-$, 323.18 $[M\text{-}H\text{-}120\text{-}146(rham)\text{-}18(H_2O)]^-$, and 308 $[M\text{-}H\text{-}120\text{-}146(rham)\text{-}18(H_2O)\text{-}CH_3]^-$. The fragmentation pattern corresponds to the sequential loss of a *C*-hexoside and an *O*-rhamnoside. The lack of a fragment characteristic of 6-*C*-hexosides at *m*/*z* 517 $[M\text{-}H\text{-}90]^-$ confirms that the *C*-hexosides are linked to the aglycone at the 8-*C* position. Based on these findings, metabolite **55** was identified as chrysoeriol 8-*C*-hexoside *O*-rhamnoside.[45]

We identified mono- and di-*O*-pinocembrin hexosides for the first time in leaves and fruits of *P. aculeata*. These compounds were tentatively characterized based on their precursor ions, detected at *m*/*z* (416.98, $R_t = 7.953$) and *m*/*z* (579.01, $R_t = 6.365$), respectively. The key diagnostic fragmentation pattern for pinocembrin derivatives was observed in both compounds **64** and **57**, marked by a prominent ion at *m*/*z* 255.05/254.98 characteristic for pinocembrin aglycone. In the MS analysis of compound **64**, the loss of a hexose unit produced a characteristic daughter ion at *m*/*z* 255.05 $[M\text{-}H\text{-}162(gl)]^-$, confirming its identity as pinocembrin-*O*-hexoside. Similarly, the MS analysis of compound **57** revealed the sequential loss of hexose moieties, evidenced by diagnostic daughter ions at *m*/*z* 417.09 $[M\text{-}H\text{-}162(hex)]^-$ and *m*/*z* 254.98 $[M\text{-}H\text{-}324(dihex)]^-$, confirming its characterization as pinocembrin-di-*O*-hexoside. The pinocembrin aglycone (**85**) was assigned in all examined parts at *m*/*z* (255.12, $R_t = 8.256$).

3.2.2.2.3. Detection of non-colored flavonoids (flavan-3-ols). Catechin (**74**), and (+)-gallocatechin (**75**) were viewed as a cluster comprising two linked nodes (C) (Fig. 3). The results presented in Table 1 highlight the relative abundance of base ions

detected for the first time exclusively in fruit at *m*/*z* 451.12, 289.00, and 305.00 in negative ion mode. These ions serve as key markers for the identification of catechin hexosides (**73**), catechin (**74**), and (+)-gallocatechin (**75**), respectively.

3.2.2.2.4. Flavanone-based derivatives. The fragmentation behavior of naringenin derivatives in a butanol extract is defined by the neutral loss of pseudo-molecular ions $[M-H]^-$, producing a dominant fragment ion at *m*/*z* 271, corresponding to the naringenin aglycone. Additional fragment ions include *m*/*z* 299.96 $[M\text{-}H\text{-}OCH_3]^-$, indicative of methoxylated naringenin (**76**) in the stem, and *m*/*z* 417.05 $[M\text{-}H\text{-}162(hex)]^-$. The ion at *m*/*z* 271.14 $[M\text{-}H\text{-}162(hex)\text{-}146(rham)]^-$ represents naringenin-*O*-hexose-*O*-rhamnoside (**78**) in the leaves, while *m*/*z* 447.06 $[M\text{-}H\text{-}146(rham)]^-$ and *m*/*z* 417.04 $[M\text{-}H\text{-}176(hex)]^-$ are characteristic of naringenin-*O*-rhamnoside-*O*-hexuornide (**79**) in leaves. Fragments at *m*/*z* 343.03 $[M\text{-}H\text{-}90]^-$ and *m*/*z* 313.07 $[M\text{-}H\text{-}120]^-$ are associated with naringenin-8-*C*-hexoside (**77**) found in both leaves and stems. These fragmentation patterns highlight the structural diversity of naringenin derivatives and their specific glycosylation and methylation modifications.[46]

3.2.2.2.5. Dihydrochalcones. The total ion current (TIC) and base peak chromatogram (BPC) analyses identified three dihydrochalcone compounds (**91–93**) with molecular ions at *m*/*z* 272.99, 434.89, and 435.01, along with distinctive fragment ions at *m*/*z* 389.17, 315.13 $[M\text{-}H\text{-}120]^-$, and 273.03 $[M\text{-}H\text{-}162(hex)]^-$, respectively.[47] These compounds, previously unreported in *P. aculeata*, were confirmed as phloretin-*C*-hexoside, phloretin-*O*-hexoside (phlorizin or nothofagin), and their aglycone at *m*/*z* 272.99.

4 Antibacterial activity

The disc diffusion test was conducted on seven microorganisms, including Gram-positive strains (*S. aureus* ATCC 29213 and *S. aureus*) and Gram-negative strains (*E. coli* ATCC 25922, *E. coli*, *P. aeruginosa* ATCC 27853, *P. aeruginosa*, and *K. pneumonia*). The control treatment (60% ethanol) showed no inhibitory activity against any of the tested microorganisms. Vancomycin (30 μg) was utilized as a positive control to assess the antibacterial efficacy of the plant extracts acting as a reference standard; it exhibited significant inhibition zones across all tested bacterial strains. The outcomes of these tests are summarized in Tables 3–5.

In the disc diffusion technique, all tested extracts exhibited significant activity against all strains at a high concentration of 2 mg mL^{-1} in comparison with the result of vancomycin (30 μg) as a positive control. The butanol extract from leaves demonstrated the strongest activity, with inhibition zones of 20.13 mm against *S. aureus* ATCC 29213, 14.42 mm against *E. coli*, and 14.35 mm against *E. coli* ATCC 25922. For the remaining strains, the inhibition zones ranged from 11 mm to 14 mm at the same concentration. The butanol extract from stems exhibited the highest activity against *E. coli* ATCC 25922 (13.17 mm), *P. aeruginosa* ATCC 27853 (13.02 mm), and *E. coli* (13.01 mm). For the other strains, the inhibition zones ranged from 9 mm to 12 mm at a concentration of 2 mg mL^{-1}. The butanol extract from fruits displayed the highest activity against *K. pneumonia* (13.41 mm), *E. coli* ATCC 25922 (13.06 mm), and *P. aeruginosa* ATCC 27853 (11.23 mm). For the remaining strains, the inhibition zones ranged from 10 mm to 11 mm at a concentration of 2 mg mL^{-1}. Among all the tested extracts, leaf extract was the most effective against all microorganisms. However, the fruits butanol extract demonstrated the strongest antibacterial activity specifically against *K. pneumonia* compared to the other extracts.

A two-fold serial dilution approach was used to determine the minimum inhibitory concentrations (MICs) of the butanol extracts from the investigated plant organs. The values ranged from 250 to 0.47 mg mL^{-1}. The experiments were run in duplicate against seven distinct bacterial strains, including Gram-positive and Gram-negative species. Table 5 shows the MIC values, represented as mean ± standard error (S.E.) (Table 6).

The results of the disk diffusion assay showed moderate inhibition zones ranging from approximately 11 to 14 mm for most extracts, indicating notable antibacterial effects. These findings were further confirmed by the MIC values, which ranged between 4.0 and 8.5 mg mL^{-1} for the majority of the tested strains. This close correlation between the two methods reflects the reliability of the antibacterial potential of the

Table 3 Antibacterial activity of butanol leaves extract on seven microorganisms by disk diffusion assay[a]

	Inhibition zone of extract (mm)				
	Leaf extract			Control (−ve/+ve)	
Microorganisms	2 mg mL^{-1}	1 mg mL^{-1}	0.5 mg mL^{-1}	60% ethanol	Vancomycin, (30 μg per disc)
(*E. coli*) ATCC25922	14.35 ± 0.80	14.13 ± 0.90	13.38 ± 1.00	0	19.3 ± 0.6
(*P. aeruginosa*) ATCC27853	14.17 ± 0.68	12.80 ± 0.80	12.05 ± 0.10	0	17.3 ± 0.4
(*S. aureus*) ATCC29213	20.13 ± 1.48	17.41 ± 0.90	14.36 ± 1.80	0	18.6 ± 0.7
E. coli	14.42 ± 0.80	11.99 ± 0.60	12.00 ± 0.50	0	18.9 ± 0.9
P. aeruginosa	11.37 ± 1.88	13.22 ± 1.30	10.62 ± 0.60	0	17.1 ± 0.5
S. aureus	12.44 ± 2.60	10.41 ± 1.50	10.02 ± 2.00	0	17.8 ± 0.9
K. pneumonia	11.10 ± 1.10	11.00 ± 1.20	10.30 ± 1.07	0	19.0 ± 0.6

[a] The 60% ethanol control treatment exhibited no inhibitory effects on any of the tested microorganisms.

Table 4 Antibacterial activity of stems extract on seven microorganisms by disk diffusion assay[a]

	Inhibition zone of extract (mm)				
	Stem extract			Control (−ve/+ve)	
Microorganisms	2 mg mL^{-1}	1 mg mL^{-1}	0.5 mg mL^{-1}	60% ethanol	Vancomycin (30 μg per disc)
(*E. coli*) ATCC25922	13.17 ± 1.80	11.99 ± 1.70	11.28 ± 0.90	0	19.3 ± 0.6
(*P. aeruginosa*) ATCC27853	13.02 ± 2.00	13.45 ± 1.40	10.11 ± 2.40	0	17.3 ± 0.4
(*S. aureus*) ATCC29213	11.58 ± 0.90	10.43 ± 0.30	8.28 ± 0.80	0	18.6 ± 0.7
E. coli	13.01 ± 1.60	11.72 ± 1.10	9.52 ± 2.00	0	18.9 ± 0.9
P. aeruginosa	10.93 ± 0.58	11.43 ± 1.00	9.32 ± 1.20	0	17.1 ± 0.5
S. aureus	11.01 ± 2.60	10.32 ± 1.50	8.12 ± 1.60	0	17.8 ± 0.9
K. pneumonia	9.40 ± 1.02	9.31 ± 2.5	12.57 ± 0.40	0	19.0 ± 0.6

[a] The 60% ethanol control treatment exhibited no inhibitory effects on any of the tested microorganisms.

Table 5 Antibacterial activity of fruits extract on seven microorganisms by disk diffusion assay[a]

	Inhibition zone of extract (mm)				
	Fruit extract			Control (−ve/+ve)	
Microorganisms	2 mg mL^{-1}	1 mg mL^{-1}	0.5 mg mL^{-1}	60% ethanol	Vancomycin (30 μg per disc)
(*E. coli*) ATCC25922	13.06 ± 1.50	12.52 ± 1.10	11.28 ± 0.90	0	19.3 ± 0.6
(*P. aeruginosa*) ATCC27853	11.23 ± 2.30	11.09 ± 2.70	10.11 ± 2.40	0	17.3 ± 0.4
(*S. aureus*) ATCC29213	10.54 ± 1.30	11.93 ± 0.50	8.28 ± 0.80	0	18.6 ± 0.7
E. coli	11.10 ± 1.80	10.98 ± 2.50	9.52 ± 2.00	0	18.9 ± 0.9
P. aeruginosa	10.90 ± 1.40	11.82 ± 1.30	9. 32 ± 1.20	0	17.1 ± 0.5
S. aureus	10.97 ± 1.60	9.33 ± 0.70	8.12 ± 1.60	0	17.8 ± 0.9
K. pneumonia	13.41 ± 0.50	12.81 ± 0.23	12.57 ± 0.40	0	19.0 ± 0.6

[a] The 60% ethanol control treatment exhibited no inhibitory effects on any of the tested microorganisms.

extracts. Specifically, leaves extract demonstrated the strongest antibacterial activity, with lower MIC values (4.0–6.0 mg mL^{-1}) against both standard and clinical isolates of *E. coli* and *P. aeruginosa*, consistent with their relatively larger inhibition zones observed in the disk diffusion assay. Similarly, the MIC of 1.5 mg mL^{-1} against *S. aureus* (ATCC29213) supports the large inhibition zone (20.13 ± 1.48 mm) observed, confirming the high sensitivity of this strain to the leaves extract. The stems extract also showed effective antibacterial activity with MIC values ranging from 4.8 to 8.5 mg mL^{-1}. The inhibition zones recorded for the stems extract, although slightly smaller compared to the leaves extract, were still significant and aligned with the MIC data. Notably, the MIC against *K. pneumoniae* reached 8.5 mg mL^{-1}, matching the smaller inhibition zone (9.40 ± 1.02 mm) obtained for this bacterium. Fruits extract exhibited comparable MIC values (4.6–7.1 mg mL^{-1}), which corresponded well with the observed inhibition zones in the disk diffusion assay. In particular, *K. pneumoniae* showed a relatively low MIC value (4.6 ± 0.3 mg mL^{-1}) against fruits extract, consistent with a moderate inhibition zone size. Overall, the data revealed that all parts of the plant possess notable antibacterial activities, with leaves extract generally showing the highest potency.[13,14] The consistency between the disk diffusion and MIC results emphasizes the potential of the butanol extracts as promising antibacterial agents. The relatively low MIC values obtained, especially for *S. aureus*, *E. coli*, and *P. aeruginosa*, further highlight the efficacy of these extracts and suggest their possible application in the development of new antimicrobial agents.

Table 6 MIC of butanol extracts from examined plant parts against seven microorganisms by microbroth dilution technique[a]

	MIC mg mL^{-1}		
Microorganism	Leaf extract	Stem extract	Fruit extract
E. coli ATCC 25922	4.2 ± 0.1	4.8 ± 0.3	4.9 ± 0.2
P. aeruginosa ATCC27853	4.5 ± 0.3	4.9 ± 0.2	5.7 ± 0.4
S. aureus ATCC29213	1.5 ± 0.2	5.5 ± 0.4	7.1 ± 0.1
E. coli (clinical)	4.0 ± 0.1	4.9 ± 0.3	6.0 ± 0.3
P. aeruginosa	5.5 ± 0.1	6.9 ± 0.3	6.8 ± 0.4
S. aureus	5.1 ± 0.3	6.0 ± 0.3	6.5 ± 0.2
K. pneumoniae	6.0 ± 0.3	8.5 ± 0.2	4.6 ± 0.3

[a] Note: values are expressed in (mg mL^{-1}).

The MIC and disk diffusion findings show that *P. aculeata* leaves and stems extracts have equivalent antibacterial activity, which is most likely owing to identical phytochemical

composition. In contrast, the fruits extract had reduced effectiveness, indicating a different profile of bioactive components.

The butanol extracts showed strong antibacterial effects because they contain a lot of different chemicals, including important secondary metabolites found through LC-MS analysis. Several antibacterial compounds have been detected in *P. aculeata* extracts, as reported by Hosseini Doust 2018.[48] The primary components of butanol extracts include *O*-caffeoylquinic acid, caffeic acid, gallic acid, dihydrokaempferol-6-*C*-hexoside, quercetin-3-*O*-rutinoside, dimethylquercetin-7-*O*-pentoside-8-*C*-hexoside, kaempferol, luteolin-8-*C*-hexoside-*O*-rhamnoside, luteolin-8-*C*-hexoside (orientin), naringenin-8-*C*-hexoside, apigenin, acacetin, and pinoresinol. The antibacterial effects of all these components are outlined below. Various studies have highlighted the inhibitory effects of plant flavonoid-rich extracts and pure flavonoids against certain pathogenic bacteria. It has also been noted that the presence of hydroxyl groups at different positions on the A and B rings of flavonoids enhance their antibacterial activity. Hydroxyl groups (OH) at positions 5, 3′, and 4′ on the A and B rings, along with a methoxy group (OMe) at C-5′, have demonstrated significant activity against *S. aureus*. In the A ring, several studies have confirmed that the combined hydroxylation at positions 5 and 7 plays a crucial role in the antibacterial activity of flavonols against *S. aureus* strains.[49] Additionally, research by Bitchagno *et al.*, 2015 (ref. 50) revealed that tetraflavonoids lacking hydroxyl groups on the C ring exhibit moderate activity against *E. coli*. The *O*-caffeoylquinic acid isomers have demonstrated antibacterial activity against *S. aureus*, *E. coli*, *P. aeruginosa*, and *K. pneumonia*.[51] The fruit's strong antimicrobial effect against *K. pneumonia* is attributed to the high abundance of *O*-caffeoylquinic acid isomers in its extract. Caffeic acid has been identified as having antibacterial properties when tested both individually and in combination with plant extracts, showing activity against clinical strains of *S. aureus*.[52,53] Additionally, studies have revealed that gallic acid and its methyl ester exhibit antibacterial activity against *S. aureus* and *E. coli*.[54] Flavonols, including kaempferol, quercetin, myricetin, and their derivatives, have demonstrated effectiveness against *S. aureus*, *E. coli*, and *K. pneumonia* strains.[55] Similarly, flavones such as luteolin, naringenin, apigenin, acacetin, diosmetin, and their isomers exhibit antibacterial properties against *S. aureus* and *E. coli*.[49] Leaves extract stands out as having the strongest antibacterial activity, likely due to the high abundance of luteolin and kaempferol derivatives in its composition.

5 Conclusion

The butanol extracts derived from leaves, stems, and fruits of *P. aculeata* presented notable antibacterial activity against seven bacterial strains, including both Gram-positive (*Staphylococcus aureus* ATCC 29213 and *S. aureus*) and Gram-negative (*Escherichia coli* ATCC 25922, *E. coli*, *Pseudomonas aeruginosa* ATCC 27853, *P. aeruginosa*, and *Klebsiella pneumoniae*). This antimicrobial effect is likely due to the high concentration of secondary metabolites identified through LC-MS/MS analysis, which are believed to play a pivotal role in microbial inhibition. These findings highlight the potential of *P. aculeata* as a promising source for developing natural treatments for various infectious diseases. However, further studies are required to comprehensively evaluate the safety profile and potential side effects of these extracts prior to their medicinal application.

Data availability

The authors affirm that the data underpinning the findings of this research are fully accessible within the article.

Molecular networking: The raw data files generated from LC-ESI-MS/MS analysis were converted into mzXML format using the MS Convert tool from ProteoWizard (version 3.0.21050, **https://proteowizard.org**). Once converted, the data were uploaded to the MassIVE Data sets repository *via* WinSCP (**https://massive.ucsd.edu**). The resulting molecular network was exported as a GraphML file and visualized using a force-directed layout in Cytoscape version 3.7.1.

HPLC-ESI-MS/MS: The MS-DIAL software version 4.70 and the Fiehn HILIC library were used to identify the constituents.

Author contributions

All authors participated in all stages of this study. All authors have read and agreed to the published version of the manuscript.

Conflicts of interest

The authors declare no conflicts of interest.

Acknowledgements

The authors would like to thank M. S. Marzouk of the Chemistry of Tanning Materials and Leather Technology Department, National Research Centre, for plant phenolics and their applications.

References

1 N. A. Ali, G. H. Elsayed, S. H. Mohamed, A. S. Abd Elkarim, M. S. Aly, A. M. Elgamal, W. M. Elsayed and S. A. El-Newary, Chia seed (*Salvia hispanica*) attenuates chemically induced lung carcinomas in rats through suppression of proliferation and angiogenesis, *Pharmaceuticals*, 2024, **17**(9), 1129, DOI: **10.3390/ph17091129**.

2 A. S. Abd Elkarim and H. A. Taie, Characterization of Flavonoids from *Combretum indicum* L. Growing in Egypt as Antioxidant and Antitumor Agents, *Egypt. J. Chem.*, 2023, **66**(13), 1519–1543, DOI: **10.21608/ejchem.2023.210414.7966**.

3 A. S. Abd Elkarim, A. H. Ahmed, H. A. Taie, A. M. Elgamal and M. A. E. S. Shabana, *Synadenium grantii* hook f.: HPLC/QTOF-MS/MS tentative identification of the phytoconstituents, antioxidant, antimicrobial and antibiofilm evaluation of the aerial parts, *Rasayan J. Chem.*, 2021, **14**, 811–828, DOI: **10.31788/RJC.2021.1426165**.

4 A. M. Nagy, M. F. Abdelhameed, A. S. A. Elkarim, T. C. Sarker, A. M. Abd-ElGawad, A. I. Elshamy and A. M. Hammam, Enhancement of Female Rat Fertility *via* Ethanolic Extract from *Nigella sativa L.* (Black Cumin) Seeds Assessed *via* HPLC-ESI-MS/MS and Molecular Docking, *Molecules*, 2024, **29**(3), 735, DOI: **10.3390/molecules29030735**.

5 A. S. Abd Elkarim, S. H. Mohamed, N. A. Ali, G. H. Elsayed, M. S. Aly, A. M. Elgamal, W. M. Elsayed and S. A. El-Newary, The Phytochemical Profile of the Petroleum Ether Extract of Purslane Leaves and Its Anticancer Effect on 4-(Methylnitrosamino)-1-(3-pyridyl)-1-buta-4 None (NNK)-Induced Lung Cancer in Rats, *Int. J. Mol. Sci.*, 2024, **25**(23), 13024, DOI: **10.3390/ijms252313024**.

6 N. Srikacha and K. Ratananikom, Antibacterial activity of plant extracts in different solvents against pathogenic bacteria: an: *in vitro*: experiment, *J. Acute Dis.*, 2020, **9**(5), 223–226, DOI: **10.4103/2221-6189.291288**.

7 M. W. A. Halmy, A. A. Yasien and M. G. Sheded, *Parkinsonia aculeata* L. recorded as alien species in natural habitats of Egypt: potential for naturalization, invasion or utilization, *Phytotaxa*, 2024, **641**(2), 112–124, DOI: **10.11646/phytotaxa.641.2.3**.

8 H. A. Hassanin, A. Taha, H. I. M. Ibrahim, E. A. Ahmed, H. Mohamed and H. Ahmed, Cytotoxic activity of bimetallic Ag@Se green synthesized nanoparticles using Jerusalem Thorn (*Parkinsonia aculeata*), *Front. Chem.*, 2024, **12**, 1343506, DOI: **10.3389/fchem.2024.1343506**.

9 S. Abdelaziz, H. M. Al Yousef, A. S. Al-Qahtani, W. H. Hassan, O. I. Fantoukh and M. A. El-Sayed, Phytochemical profile, antioxidant and cytotoxic potential of *Parkinsonia aculeata* L. growing in Saudi Arabia, *Saudi Pharm. J.*, 2020, **28**(9), 1129–1137, DOI: **10.1016/j.jsps.2020.08.001**.

10 W. H. Hassan, S. Abdelaziz and H. M. Al Yousef, Chemical composition and biological activities of the aqueous fraction of *Parkinsonea aculeata L.* growing in Saudi Arabia, *Arabian J. Chem.*, 2019, **12**(3), 377–387, DOI: **10.1016/j.arabjc.2018.08.003**.

11 O. Awwad, N. Aboalhaija, I. Abaza, R. Abbassi, M. H. Kailani, H. Al-Jaber and F. U. Afifi, Chromatographic (LC-MS and GC-MS) and biological (antiproliferative) evaluation of a naturalized plant in Jordan: *Parkinsonia aculeata* L., *J. Herb. Med.*, 2023, **39**, 100659, DOI: **10.1016/j.hermed.2023.100659**.

12 K. K. Zambare, A. A. Kondapure, K. V. Reddy, A. B. Thalkari, P. N. Karwa, Y. P. Nikam, A. A. Gholkar and R. B. Darade, A systematic review on potential pharmacological applications of *Parkinsonia aculeata*, *Res. J. Pharm. Technol.*, 2021, **14**(3), 1767–1770, DOI: **10.5958/0974-360X.2021.00314.0**.

13 N. S. Younas, I. Ali, H. Ashraf and N. T. Bukhari, Antimicrobial potential of ethanolic leaf extracts of *Parkinsonia aculeate* using response surface methodology, *Biol. Clin. Sci. Res. J.*, 2022, **160**, 1.

14 C. Revanayya Swami, S. Darshan Lokhande and G. Rakesh Gaikwad, A brief review on pharmacological significance of *Parkinsonia aculeata*, *Int. J. Creat. Res. Thoughts*, 2023, **11**(10), b923.

15 M. R. M. Askar, Bacterial responses to Ephedra aphylla stem extract and green-synthesized Ag-TiO_2 and Ag-SeO_2 core/shell nanocomposites: unveiling antimicrobial and antioxidant properties, *RSC Adv.*, 2025, **15**(17), 13152–13171, DOI: **10.1039/d5ra00936g**.

16 R. M. Ibrahim, B. M. Eltanany, L. Pont, F. Benavente, S. A. ElBanna and A. M. Otify, Unveiling the functional components and antivirulence activity of *mustard* leaves using an LC-MS/MS, molecular networking, and multivariate data analysis integrated approach, *Food Res. Int.*, 2023, **168**, 112742, DOI: **10.1016/j.foodres.2023.112742**.

17 M. N. Khalil, S. M. Afifi, B. M. Eltanany, L. Pont, F. Benavente, S. M. El-Sonbaty and M. S. Sedeek, Assessment of the effect of drying on *Brassica* greens *via* a multiplex approach based on LC-QTOF-MS/MS, molecular networking, and chemometrics along with their antioxidant and anticancer activities, *Food Res. Int.*, 2024, **180**, 114053, DOI: **10.1016/j.foodres.2024.114053**.

18 A. Mehmood, S. Javid, M. F. Khan, K. S. Ahmad and A. Mustafa, *In vitro* total phenolics, total flavonoids, antioxidant and antibacterial activities of selected medicinal plants using different solvent systems, *BMC Chem.*, 2022, **16**(1), 64, DOI: **10.1186/s13065-022-00858-2**.

19 K. M. Patel, B. B. Parmar, K. A. Sadariya and S. K. Bhavsar, Assessment of *in vitro* antibacterial activity and MIC of *cinnamon* bark powder ethanolic and aqueous extracts against bacteria, *J. Phytopharm.*, 2022, **11**(5), 324–329, DOI: **10.31254/phyto.2022.11502**.

20 D. Escobar-Avello, J. Lozano-Castellón, C. Mardones, A. J. Pérez, V. Saéz, S. Riquelme, D. von Baer and A. Vallverdú-Queralt, Phenolic profile of *grape canes*: novel compounds identified by LC-ESI-LTQ-orbitrap-MS, *Molecules*, 2019, **24**(20), 3763, DOI: **10.3390/molecules24203763**.

21 P. K. Yılmaz, A. Ertaş, M. Akdeniz, M. K. Avcı and U. Kolak, Chemical compositions by LC-MS/MS and GC-MS and biological activities of *Chenopodium album* subsp. album var. microphyllum, *Ind. Crops Prod.*, 2019, **141**, 111755, DOI: **10.1016/j.indcrop.2019.111755**.

22 P. Ambigaipalan, A. C. de Camargo and F. Shahidi, Identification of phenolic antioxidants and bioactives of *pomegranate* seeds following juice extraction using HPLC-DAD-ESI-MSn, *Food Chem.*, 2017, **221**, 1883–1894, DOI: **10.1016/j.foodchem.2016.10.058**.

23 F. Khallouki, I. Ricarte, A. Breuer and R. W. Owen, Characterization of phenolic compounds in mature Moroccan Medjool *date palm* fruits (*Phoenix dactylifera*) by HPLC-DAD-ESI-MS, *J. Food Compos. Anal.*, 2018, **70**, 63–71, DOI: **10.1016/j.jfca.2018.03.005**.

24 W. A. El-Kashak, A. F. Essa, M. F. Abdelhameed, Y. H. Ahmed, A. S. Abd Elkarim, M. M. Elghonemy, B. M. Ibrahim, A. H. Gaara, T. K. Mohamed and A. I. Elshamy, Unveiling the neuroprotective potential of *Ipomoea carnea* ethanol extract *via* the modulation of tau and β-secretase pathways in $AlCl_3$-induced memory impairment in rats in relation to its phytochemical

profiling, *Inflammopharmacology*, 2025, 1–26, DOI: 10.1007/s10787-025-01687-0.

25 K. Kramberger, D. Barlič-Maganja, D. Bandelj, A. Baruca Arbeiter, K. Peeters, A. Miklavčič Višnjevec and Z. Jenko Pražnikar, HPLC-DAD-ESI-QTOF-MS determination of bioactive compounds and antioxidant activity comparison of the hydroalcoholic and water extracts from two *Helichrysum italicum* species, *Metabolites*, 2020, **10**(10), 403, DOI: 10.3390/metabo10100403.

26 M. Yang, J. Li, C. Zhao, H. Xiao, X. Fang and J. Zheng, LC-Q-TOF-MS/MS detection of food flavonoids: principle, methodology, and applications, *Crit. Rev. Food Sci. Nutr.*, 2023, **63**(19), 3750–3770.

27 E. J. Llorent-Martínez, V. Spínola, S. Gouveia and P. C. Castilho, HPLC-ESI-MSn characterization of phenolic compounds, terpenoid saponins, and other minor compounds in *Bituminaria bituminosa*, *Ind. Crops Prod.*, 2015, **69**, 80–90, DOI: 10.1016/j.indcrop.2015.02.014.

28 T. Du, Y. Wang, H. Xie, D. Liang and S. Gao, Fragmentation Patterns of Phenolic *C*-Glycosides in Mass Spectrometry Analysis, *Molecules*, 2024, **29**(13), 2953, DOI: 10.22541/au.172499499.91739325/v1.

29 T. Du, Y. Wang, H. Xie, D. Liang and S. Gao, Fragmentation Patterns of Dietary Phenolic *C*-Glycosides in Mass Spectrometry Analysis, available at SSRN 4604720.

30 P. Geng, M. Zhang, J. M. Harnly, D. L. Luthria and P. Chen, Use of fuzzy chromatography mass spectrometric (FCMS) fingerprinting and chemometric analysis for differentiation of whole-grain and refined wheat (*T. aestivum*) flour, *Anal. Bioanal. Chem.*, 2015, **407**, 7875–7888, DOI: 10.1007/s00216-015-9007-5.

31 P. Geng, J. Sun, M. Zhang, X. Li, J. M. Harnly and P. Chen, Comprehensive characterization of *C*-glycosyl flavones in wheat (*Triticum aestivum* L.) germ using UPLC-PDA-ESI/HRMSn and mass defect filtering, *J. Mass Spectrom.*, 2016, **51**(10), 914–930, DOI: 10.1002/jms.3803.

32 Z. Benayad, C. Gómez-Cordovés and N. E. Es-Safi, Identification and quantification of flavonoid glycosides from fenugreek (*Trigonella foenum-graecum*) germinated seeds by LC-DAD-ESI/MS analysis, *J. Food Compos. Anal.*, 2014, **35**(1), 21–29, DOI: 10.1016/j.jfca.2014.04.002.

33 S. A. El-Newary, A. S. Abd Elkarim, N. A. Abdelwahed, E. A. Omer, A. M. Elgamal and W. M. ELsayed, *Chenopodium murale* Juice Shows Anti-Fungal Efficacy in Experimental Oral Candidiasis in Immunosuppressed Rats in Relation to Its Chemical Profile, *Molecules*, 2023, **28**(11), 4304, DOI: 10.3390/molecules28114304.

34 L. Zhuan-Hong, G. Han, X. Wen-Bin, G. Juan, L. Xin, A. Mireguli and H. Da-Jun, Rapid Identification of flavonoid constituents directly from PTP1B inhibitive extract of *raspberry* (*daeus* L.) leaves by HPLC-ESI-QTOF-MS-MS, *J. Chromatogr. Sci.*, 2016, **54**, 805–810Z.

35 Y. Qin, B. Gao, H. Shi, J. Cao, C. Yin, W. Lu, L. Yu and Z. Cheng, Characterization of flavonol mono-, di-, tri-and tetra-*O*-glycosides by ultra-performance liquid chromatography-electrospray ionization-quadrupole time-of-flight mass spectrometry and its application for identification of flavonol glycosides in *Viola tianschanica*, *J. Pharm. Biomed. Anal.*, 2017, **142**, 113–124, DOI: 10.1016/j.jpba.2017.05.007.

36 R. Pascale, M. A. Acquavia, T. R. Cataldi, A. Onzo, D. Coviello, S. A. Bufo, L. Scrano, R. Ciriello, A. Guerrieri and G. Bianco, Profiling of quercetin glycosides and acyl glycosides in sun-dried peperoni di Senise peppers (*Capsicum annuum* L.) by a combination of LC-ESI (−)-MS/MS and polarity prediction in reversed-phase separations, *Anal. Bioanal. Chem.*, 2020, **412**, 3005–3015, DOI: 10.1007/s00216-020-02547-2.

37 B. Huang, F. Chen, X. Zhang, Y. Hu, Y. Zhang, L. Chen, Y. Meng and P. Wen, A fragmentation study of disaccharide flavonoid *C*-glycosides using triple quadrupole mass spectrometry and its application for identification of flavonoid *C*-glycosides in *Odontosoria chinensis*, *Rapid Commun. Mass Spectrom.*, 2025, **39**(2), e9936, DOI: 10.1002/rcm.9936.

38 S. Sharma and A. P. Vig, Preliminary phytochemical screening and *in vitro* antioxidant activities of *Parkinsonia aculeata* Linn., *BioMed Res. Int.*, 2014, **2014**(1), 756184, DOI: 10.1155/2014/756184.

39 Y. Wang, M. Gu, J. Mao, J. Liu, S. Fan, H. Zhang, H. Bu and Q. Liu, Phytochemical study: fragmentation patterns of flavonoid-*C*-glycosides in the enriched flavonoids from *corn* silk using high-efficiency ultra-high-performance liquid chromatography combined with quadrupole time-of-flight mass spectrometry, *Sep. Sci. plus*, 2024, **7**(2), 2300156, DOI: 10.1002/sscp.202300156.

40 M. E. Karar and N. J. J. C. B. T. Kuhnert, UPLC-ESI-Q-TOF-MS/MS characterization of phenolics from *Crataegus monogyna* and *Crataegus laevigata* (Hawthorn) leaves, fruits and their herbal derived drops (Crataegutt Tropfen), *J. Chem. Biol. Ther*, 2015, **1**(102), 2572–0406, DOI: 10.4172/2572-0406.1000102.

41 A. Wojakowska, J. Perkowski, T. Góral and M. Stobiecki, Structural characterization of flavonoid glycosides from leaves of wheat (*Triticum aestivum* L.) using LC/MS/MS profiling of the target compounds, *J. Mass Spectrom.*, 2013, **48**(3), 329–339, DOI: 10.1002/jms.3160.

42 G. Domínguez-Rodríguez, M. C. García, M. Plaza and M. L. Marina, Revalorization of *Passiflora* species peels as a sustainable source of antioxidant phenolic compounds, *Sci. Total Environ.*, 2019, **696**, 134030, DOI: 10.1016/j.scitotenv.2019.134030.

43 A. Brito, J. E. Ramirez, C. Areche, B. Sepúlveda and M. J. Simirgiotis, HPLC-UV-MS profiles of phenolic compounds and antioxidant activity of fruits from three *citrus* species consumed in Northern Chile, *Molecules*, 2014, **19**(11), 17400–17421, DOI: 10.3390/molecules191117400.

44 J. Cao, C. Yin, Y. Qin, Z. Cheng and D. Chen, Approach to the study of flavone di-*C*-glycosides by high performance liquid chromatography-tandem ion trap mass spectrometry and its application to characterization of flavonoid composition in *Viola yedoensis*, *J. Mass Spectrom.*, 2014, **49**(10), 1010–1024, DOI: 10.1002/jms.3413.

45 M. A. El-Sayed, A. A. Al-Gendy, D. I. Hamdan and A. M. El-Shazly, Phytoconstituents, LC-ESI-MS profile, antioxidant and antimicrobial activities of *Citrus* x*limon* L. Burm. f. cultivar variegated pink lemon, *J. Pharmaceut. Sci. Res.*, 2017, **9**(4), 375.

46 Z. H. Li, H. Guo, W. B. Xu, J. Ge, X. Li, M. Alimu and D. J. He, Rapid identification of flavonoid constituents directly from PTP1B inhibitive extract of *raspberry* (*Rubus idaeus* L.) leaves by HPLC-ESI-QTOF-MS-MS, *J. Chromatogr. Sci.*, 2016, **54**(5), 805–810, DOI: **10.1093/chromsci/bmw016**.

47 P. Mena, L. Calani, C. Dall'Asta, G. Galaverna, C. García-Viguera, R. Bruni, A. Crozier and D. Del Rio, Rapid and comprehensive evaluation of (poly) phenolic compounds in *pomegranate* (*Punica granatum* L.) juice by UHPLC-MSn, *Molecules*, 2012, **17**(12), 14821–14840, DOI: **10.3390/molecules171214821**.

48 S. R. Hosseini Doust, F. Mirzaee, N. Dakhili, M. Salehi and M. Razzaghi-Abyaneh, Antimicrobial activities of *Parkinsonia aculeata* and *Prosopiskoelziana* extracts against pathogenic fungi and bacteria (*Staphylococcus aureus*, *S. epidermidis*, *S. pyogenes*, *Pseudomonas aeruginosa*, *Escherichia coli*, *Aspergillus niger*, *A. flavus*, *A. fumigatus*, *F. solani*, *Microsporum gypseum*, *M. mcanis*, *Trichophyton verrucosum*, *T. rubrum* and *Candida albicans*), *Asian J. Pharm. Health Sci.*, 2018, **6**(1), 29–37.

49 F. Farhadi, B. Khameneh, M. Iranshahi and M. Iranshahy, Antibacterial activity of flavonoids and their structure–activity relationship: an update review, *Phytother. Res.*, 2019, **33**(1), 13–40, DOI: **10.1002/ptr.6208**.

50 G. T. M. Bitchagno, L. Sama Fonkeng, T. K. Kopa, M. F. Tala, H. Kamdem Wabo, C. B. Tume, P. Tane and J. R. Kuiate, Antibacterial activity of ethanolic extract and compounds from fruits of *Tectona grandis* (Verbenaceae), *BMC Complementary Altern. Med.*, 2015, **15**, 1–6, DOI: **10.1186/s12906-015-0790-5**.

51 E. Bajko, M. Kalinowska, P. Borowski, L. Siergiejczyk and W. Lewandowski, 5-*O*-Caffeoylquinic acid: a spectroscopic study and biological screening for antimicrobial activity, *Food Sci. Technol.*, 2016, **65**, 471–479, DOI: **10.1016/j.lwt.2015.08.024**.

52 M. Kępa, M. Miklasińska-Majdanik, R. D. Wojtyczka, D. Idzik, K. Korzeniowski, J. Smoleń-Dzirba and T. J. Wąsik, Antimicrobial potential of caffeic acid against Staphylococcus aureus clinical strains, *BioMed Res. Int.*, 2018, **2018**(1), 7413504, DOI: **10.1155/2018/7413504**.

53 F. Khan, N. I. Bamunuarachchi, N. Tabassum and Y. M. Kim, Caffeic acid and its derivatives: antimicrobial drugs toward microbial pathogens, *J. Agric. Food Chem.*, 2021, **69**(10), 2979–3004, DOI: **10.1021/acs.jafc.0c07579**.

54 V. N. Lima, C. D. Oliveira-Tintino, E. S. Santos, L. P. Morais, S. R. Tintino, T. S. Freitas, Y. S. Geraldo, R. L. Pereira, R. P. Cruz, I. R. Menezes and H. D. Coutinho, Antimicrobial and enhancement of the antibiotic activity by phenolic compounds: gallic acid, caffeic acid and pyrogallol, *Microb. Pathog.*, 2016, **99**, 56–61, DOI: **10.1016/j.micpath.2016.08.004**.

55 M. Lotfaliani, S. A. Ayatollahi, F. Kobarfard, M. B. Majnooni, A. Mirzaei, M. Ghanadian and M. H. Farzaei, Flavonoids Isolated From *Delphinium semibarbatum* Flowering Aerial Parts With Their Antibacterial, Antibiofilm, and Antiswarming Activity Against *Proteus mirabilis* and *Staphylococcus aureus*, *J. Food Biochem.*, 2024, **2024**(1), 9994944, DOI: **10.1155/jfbc/9994944**.